THESIS FOR THE DEGREE OF DOCTOR OF PHILOSOPHY
IN
THERMO AND FLUID DYNAMICS

Methodologies for RANS-LES interfaces in turbulence-resolving simulations

by

SEBASTIAN ARVIDSON

Department of Mechanics and Maritime Sciences
Division of Fluid Dynamics
CHALMERS UNIVERSITY OF TECHNOLOGY
Gothenburg, Sweden 2017

Methodologies for RANS-LES interfaces in turbulence-resolving simulations
SEBASTIAN ARVIDSON
ISBN 978-91-7597-583-2

Doktorsavhandlingar vid Chalmers tekniska högskola
Ny serie nr. 4264
ISSN 0346-718X

Department of Mechanics and Maritime Sciences
Division of Fluid Dynamics
Chalmers University of Technology
SE-412 96 Gothenburg
Sweden
Telephone: +46 (0)31-772 1000

This document was typeset using LaTeX

Printed at Chalmers Reproservice
Gothenburg, Sweden 2017

Methodologies for RANS-LES interfaces in turbulence-resolving simulations

Sebastian Arvidson

Department of Mechanics and Maritime Sciences
Division of Fluid Dynamics
Chalmers University of Technology

Abstract

Hybrid Reynolds-Average Navier-Stokes (RANS)-Large-Eddy Simulations (LES) techniques are now seen by the aeronautical industry as the most promising turbulence-resolving approaches for complex high-Reynolds-number turbulent flows with regard to cost and accuracy. However, connecting RANS and LES simulated flows is a challenging task and needs special attention in order to increase simulation robustness and accuracy.

This thesis presents a new low-Reynolds-number $k-\omega$ based zonal hybrid RANS-LES turbulence model with which novel interface methodologies for connecting RANS and LES regions are explored. The emphasis of the work reported in the thesis is on RANS-LES interface techniques for grey-area mitigation and reduction of log-layer mismatch since these are the two most important issues to resolve in hybrid RANS-LES modeling in order to meet industry requirements for robustness and accuracy.

The proposed hybrid RANS-LES model was applied to Decaying Homogeneous Isotropic Turbulence (DHIT) and channel flow for calibration purposes. It was concluded from the simulations of fully developed channel flow that a wall distance based LES length scale was superior in reducing the log-layer mismatch compared to other LES length scales discussed in the literature.

It was shown from simulations of spatially developing boundary layer flow and flow over a wall-mounted hump that a RANS-LES interface technique combining commutation terms, introduced in the k and ω equations to reduce the turbulent viscosity, and synthetic turbulent fluctuations substantially mitigates the grey area as compared to commonly used RANS-LES interface methods and gives results that are in good agreement with experimental data.

In simulations of a plane mixing layer flow, commutation terms were introduced in the k, ω and momentum equations in order to represent the transfer of energy between modeled and resolved turbulent scales at the wall-normal RANS-LES interface, located at the trailing edge of the flat plate. It was found that the commutation terms in the momentum equations are able to trigger the equations to resolve turbulence, thus mitigating the RANS-to-LES transition region and improving the prediction of the resolved turbulent stresses. These were in good agreement with experimental data.

Moreover, the proposed hybrid RANS-LES model has been successfully used to simulate a transonic flow in a rectangular duct with shock-induced corner flow separations.

Keywords: Hybrid RANS-LES, zonal RANS-LES, embedded LES, RANS-LES interfaces, grey-area mitigation, log-layer mismatch, LES, LES length scale, aeronautics

To my family.

Acknowledgements

First of all, I would like to express my sincere gratitude to my supervisors, Lars Davidson and Shia-Hui Peng, who gave me the opportunity to explore the field of turbulence modeling. I would very much like to thank you for always sharing your deep knowledge with me, always being supportive and always contributing with your positive thinking. I am also very thankful for all interesting, inspiring and fruitful discussions we have had during the years.

Many thanks go to Per Weinerfelt, who has been my supervisor at Saab Aeronautics, for all your help, support and valuable and constructive discussions. Your knowledge in mathematics, computational fluid dynamics and related topics has been invaluable.

I would like to thank my colleagues at Chalmers, who always contributed to an enjoyable atmosphere at lunches, coffee breaks and in the daily research work. Special thanks to Bastian N., Mohammad E. and Jon-Anders B. for sharing your thoughts and your contributions to enjoyable and interesting discussions. Thanks Ulla for your guidance through the administration.

Furthermore, I would like to thank my colleagues at Saab Aeronautics for always contributing to a pleasant working environment and for all our inspiring discussions about aircraft, aero-engines, simulations techniques and other interesting technical stuff. I would like to give my special thanks to Michael S. for providing your great support, inspiring discussions and your honest interest in this thesis work. Thanks Magnus D., Magnus B. and Hans-Peter M., who made my work as an industrial PhD student possible and thereby have given me lots of inspiration for my future work at Saab.

Many thanks to my dear friends with whom I share this journey. We have many memorable moments together, which have contributed to make this thesis work possible.

A big, big hug to my father, mother and sisters, you are always there for me, support me and have always encouraged me to do this. Without you, your ground support and your open hearts, the work for this thesis would not have been possible. You are invaluable! Many thanks to my grandmother Bibbi, who is a great fan. You always provide me with your strengthening love and your support!

This work has been conducted within the Swedish National Aviation Engineering Research Programme (NFFP), projects NFFP5-MADEF (2009-01346) and NFFP6-MIAU (2013-01209), funded by VINNOVA, FMV and the Swedish Armed Forces together with Saab Aeronautics. Moreover, the financial support of SNIC (Swedish National Infrastructure for Computing) for computer time at NSC (National Supercomputer Center) and C^{3}SE (Chalmers Center for Computational Science and Engineering) are gratefully acknowledged.

List of publications

This thesis consists of an extended summary and the following appended papers:

Paper A S. Arvidson, S.-H. Peng, and L. Davidson. "Feasibility of Hybrid RANS-LES of Shock/Boundary-Layer Interaction in a Duct". *Progress in Hybrid RANS-LES Modelling*. Ed. by F. S. et al. Vol. 117. NNFM. Springer, 2012, pp. 245–256

Paper B S. Arvidson, L. Davidson, and S.-H. Peng. *Hybrid RANS-LES Modeling Using a Low-Reynolds-Number $k-\omega$ Based Model*. AIAA paper 2014-0225, National Harbour, Maryland. 2014

Paper C S. Arvidson, S.-H. Peng, and L. Davidson. "Prediction of Transonic Duct Flow Using a Zonal Hybrid RANS-LES Modeling Approach". *Progress in Hybrid RANS-LES Modelling*. Ed. by S. G. et al. Vol. 130. NNFM. Springer, 2015, pp. 229–241

Paper D S. Arvidson, L. Davidson, and S.-H. Peng. Hybrid Reynolds-Averaged Navier-Stokes/Large-Eddy Simulation Modeling Based on a Low-Reynolds-Number $k-\omega$ Model. *AIAA Journal* **54** (2016), pp. 4032–4037. URL: `http://dx.doi.org/10.2514/1.J054179`

Paper E S. Arvidson, L. Davidson, and S.-H. Peng. "Grey-area mitigation using commutation terms at the interfaces in hybrid RANS-LES modeling". *To be published in Progress in Hybrid RANS-LES Modelling*. NNFM. Springer, 2017

Paper F S. Arvidson, L. Davidson, and S.-H. Peng. *Hybrid RANS-LES interface methods for grey-area mitigation in turbulence-resolving simulations*. Research report 2017:03. Applied Mechanics, Chalmers University of Technology, 2017

Division of work

All papers were written by S. Arvidson, who also developed the proposed hybrid RANS-LES model with guidance provided by Prof. L. Davidson and Prof. S-H. Peng. The model was implemented in the CALC-LES and Edge flow solvers by S. Arvidson. The wall-normal RANS-LES interface methodologies, with commutation terms in the k and ω equations, used in papers D-F were provided by Prof. L. Davidson but were adapted and fine-tuned by S. Arvidson for the computed flow cases and the turbulence model used. S. Arvidson developed and implemented the commutation terms in the momentum equations at the wall-normal interface. The wall-parallel RANS-LES interface methodologies were developed and implemented by S. Arvidson. S. Arvidson also performed all the simulations included in this thesis. Prof. L. Davidson has been the main supervisor for this thesis and supplied the CALC-LES flow solver. The work conducted with the flow solver Edge was mainly supervised by Prof. S-H. Peng. Both Prof. L. Davidson and Prof. S-H. Peng provided guidance and helpful discussions and helped with interpretations of results.

Contents

Part I
Extended Summary

The work presented in this thesis takes an aeronautical perspective. The simulated flows, chosen to demonstrate the proposed simulation techniques, are essential to improving the physical modeling of flows in aeronautical applications. The proposed modeling techniques have been demonstrated mostly for incompressible flows using an incompressible flow solver. However, as future work, the methods developed are planned to be implemented into the compressible flow solver Edge and applied to aeronautical applications.

The scope of this thesis is the development of a low-Reynolds-number $k-\omega$ based zonal hybrid RANS-LES method and novel RANS-LES interface methodologies for grey-area mitigation and reduction of the log-layer mismatch. Attention is paid to the two latter issues since these are the most important to resolve in hybrid RANS-LES modeling in order to meet industry requirement for robustness and accuracy.

The development of the proposed hybrid RANS-LES method is motivated by the outcome of paper A. It was concluded in the work reported that enhanced hybrid RANS-LES modeling was needed to improve the prediction of the analyzed shock/boundary-layer interaction flow. In paper B, the proposed zonal hybrid RANS-LES model is outlined, calibrated and validated in Decaying Homogeneous Isotropic Turbulence (DHIT) and simulations of channel flow. In paper C, the proposed model is applied to the compressible shock/boundary-layer interaction flow that was analyzed in paper A. The proposed model was applied in papers D to F to a wider range of flows with a focus on hybrid RANS-LES modeling techniques for reduction of the log-layer mismatch and the grey area.

The thesis is organized as follows. An introduction is given below to turbulent flows and how turbulent flows can be simulated. The emphasis is on hybrid RANS-LES modeling. The numerical methods used in this thesis are presented in chapter 2. The proposed hybrid RANS-LES model is presented in chapter 3, as is the proposed RANS-LES interface methodologies for grey-area mitigation and reduction of the log-layer mismatch. Chapter 4 discusses the flow cases used for calibration and validation of the proposed model. The appended papers are summarized and commented in chapter 5. Finally, chapter 6 summarizes the outcomes of the thesis work and gives some concluding remarks.

1 Introduction

This chapter introduces turbulent flows. Common simulation techniques for turbulent flows are presented with an emphasis on hybrid RANS-LES modeling, which is the primary topic of this thesis. The chapter is concluded with a section in which the motivation for this thesis work is given.

1.1 Turbulent flows

Almost all engineering flows and the flows around us are turbulent. Turbulent flows you meet in daily life are e.g. the flow in the creek you pass when you go to work, the air stream around you when you ride your bike and the rotational flow you induce in your cup when you mix the coffee and milk with your spoon at breakfast. Examples of turbulent flows associated with technical applications are e.g. flows around cars and aircraft, flows in pipes and ventilation systems.

Fluid flows can be categorized as laminar or turbulent. In order to distinguish between laminar and turbulent flows, we use one of the most essential numbers in fluid mechanics, the so-called Reynolds number.

$$Re = \frac{\rho V L}{\mu} \tag{1.1}$$

where V is a characteristic velocity scale, L is a characteristic length scale, ρ is the fluid density and μ is the fluid kinematic viscosity. The Reynolds number should be interpreted as the ratio of inertial forces to the viscous forces. For turbulent flows, the inertial forces are much larger than the viscous forces.

At which Reynolds number a flow is considered as turbulent depends on the application and how the characteristic velocity and length scales are chosen. For example, in pipe flow, the flow is considered turbulent when $Re_D = \rho U_{bulk} D/\mu > 2300$, where U_{bulk} and D are the bulk velocity and the pipe diameter, respectively. For a zero-pressure-gradient flat-plate boundary-layer flow, the flow is considered turbulent when $Re_x = \rho U_\infty L_x/\mu > 500.0000$, where L_x is the streamwise location on the plate and U_∞ is the free stream velocity.

The Reynolds number is used to indicate whether a flow is turbulent, but there is no specific definition of a turbulent flow. Nevertheless, a turbulent flow has certain characteristics.

Looking at a turbulent flow, e.g. the steam coming from the tea pot, it can be seen that it looks chaotic, irregular and three dimensional. The turbulent eddies are unsteady as they change in time. However, the turbulence is deterministic and can be mathematically described by the Navier-Stokes equations. It can also be observed that the smallest turbulent eddies are much larger than the fluid molecules and that the large turbulent eddies break down into smaller turbulent eddies and eventually dissipates (into heat). This process is called the cascade process and is shown in Fig. 1.1.

The cascade process means that the largest and most energy containing eddies represented by I in Fig. 1.1, which extract energy from the mean flow, will continuously break down to smaller eddies. The breakdown of larger eddies to smaller eddies continues until the size of the eddies reaches the Kolmogorov scale in the so-called dissipative region, represented by III in Fig. 1.1. The eddies in the dissipative region are small so that the viscous forces (stresses) kills the eddies and the kinetic energy of the small eddies are transferred to internal energy (heat). From the cascade process it is shown that the turbulence consumes energy. Hence, the turbulence has to be fed by energy from the mean flow field in order to be sustained.

Region II in Fig. 1.1, the inertial subrange, can be seen as a transfer region in wave number space between region I, with the energy-containing eddies, and region III, where

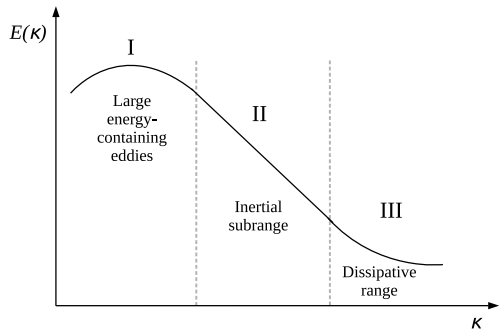

Figure 1.1: Spectrum of turbulent kinetic energy. I: Range for the largest turbulent eddies, II: Inertial subrange and III: Dissipative range, the smallest turbulent eddies. E is the energy per wave number and κ is the wave number.

the eddies dissipate into internal energy. The eddies in the inertial subrange region are independent of the eddies in regions I and III. Moreover, the difference in spatial and temporal scales between regions I and III is dependent on the Reynolds number. The larger the Reynolds number, the larger difference between the scales in the two regions. Thus, as the eddies in region II are independent of the eddies in regions I and III, the wave number range in the inertial subrange increases with an increased Reynolds number.

It should also be noted that the turbulence in the inertial subrange (II) and the dissipative region (III) is isotropic, which means that it has no preferred direction, i.e. $\overline{u'^2} = \overline{v'^2} = \overline{w'^2}$ and $\overline{u'v'} = \overline{u'w'} = \overline{v'w'} = 0$.

Even though the cascade process assumes large eddies break down into smaller eddies, it should be mentioned that a parallel, but usually much smaller, process is present where smaller eddies merge to larger eddies, so-called backscatter. Moreover, it should be mentioned that the transfer of kinetic energy to internal energy not only takes place for the dissipative scales. A small amount of kinetic energy is also transferred from the large scale eddies, present in region I, to internal energy. In the cascade process, this energy transfer is assumed to be zero.

Turbulence acts as a diffusive source in the flow and contributes to increased mixing. For example, two temperature streams will mix more rapidly in a field with strong turbulence than in a field with a lower level of turbulence. The turbulence itself is also diffusive, which means that regions of strong turbulence will spread to regions with a lower level of turbulence.

To summarize the characteristics of a turbulent flow, the following keywords are commonly used [1]: *irregularity*, *three-dimensional*, *diffusive*, *large Reynolds numbers*, *dissipative* and *continuum*.

1.2 Simulation of turbulent flows

A mathematical description of a flow is given by the Navier-Stokes equations. The local flow properties of complex flows can be determined by descritizing and solving the Navier-Stokes equations using numerical methods.

In Direct Numerical Simulations (DNS) of turbulent flows, i.e. numerically solving the Navier-Stokes equations without any modeling assumptions, the spatial and temporal discretization of the flow being analyzed must be adapted so that the full range of the spatial and the temporal scales present in the turbulent flow is resolved, as shown in Fig. 1.2. The spatial resolution needed in DNS is determined by the Kolmogorov length scale present in region III in Fig. 1.1. Furthermore, the time step needed is determined by the Kolmogorov time scale. Determined by the Kolmogorov length, time and velocity scales, the Courant-Friedrichs-Lewy (CFL) number is 1. Due to the fine grids and small time steps needed, DNS is applicable only to simple fundamental flows such as channel flow [2] and boundary layer flow [3] at low Reynolds numbers.

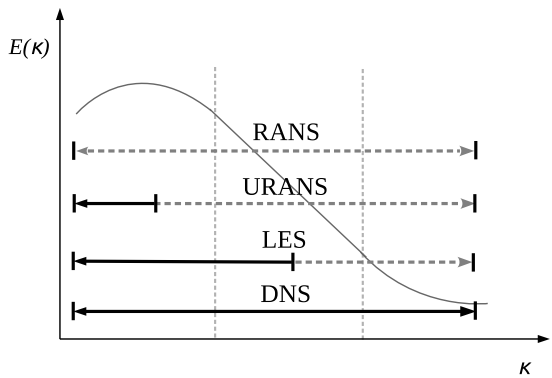

Figure 1.2: Spectrum for turbulent kinetic energy overlaid by turbulence modeling techniques with ranges of resolved and modeled turbulence. Horizontal dashed grey lines: modeled turbulence; solid black lines: resolved turbulence.

To make simulations of complex high Reynolds-number flows possible, filters are applied to the Navier-Stokes equations to reduce the spatial and temporal resolution requirements needed for DNS. The application of filters gives rise to more unknowns than the number of equations that are available, creating the so-called closure problem. These unknowns correspond to the Reynolds stress tensor that must be modeled in order to close the equation system. The models used to represent the Reynolds stress tensor are the so-called turbulence models.

Different turbulence modeling approaches are given in Table 1.1 and are presented together with the energy spectrum for turbulent kinetic energy in Fig. 1.2. The modeling approaches span from Reynolds-Average Navier-Stokes (RANS), where all turbulent scales are modeled based on mean flow quantities, to Large-Eddy Simulation (LES), where the large scale turbulence is resolved and only the turbulent scales smaller than the local grid

size (subgrid scales (SGS)) are modeled.

Table 1.1: Turbulence modeling techniques, based on [4].

Simulation technique		Turbulence resolving	Industrial readiness
RANS	Computational cost ↓ Increased accuracy	No	Yes
URANS		Yes[1]	Yes
HRLM		Yes	Limited
LES		Yes	Limited
DNS		Yes	No

[1] Only the very large turbulent scales are resolved.

RANS is based on mean flow quantities and considers the flow field to be steady state. However, unsteady RANS (URANS), i.e. RANS equations in which the transient term is retained, have the ability to resolve the largest scales of a turbulent flow, e.g. that which are caused by time dependent boundary conditions or statistically unsteady vortex shedding. The time step needed for URANS simulations is determined by low frequency phenomena and should be much larger than the turbulent time scales, which are taken care of by the turbulence model. Theoretically, in URANS simulations, the time scales of the resolved large scale turbulence should be clearly separated from the time scales of the modeled turbulence, namely the so-called scale separation. The assumption is rarely fulfilled, however.

In LES, spatial filtering is used to separate the resolved turbulence from its modeled counterpart. A flow quantity is thereby decomposed into a resolved part and an unresolved part. The amount of resolved turbulence is determined by the filter width. For finite-volume discretization codes, which are used in this thesis, the filter width is the same as the local cell size, i.e. a box filter (implicit filtering). For accurate LES predictions, the filter width should be chosen so that the cut-off wave number (κ_c) is located in the inertial sub-range, i.e. in the energy spectrum where the turbulence is said to be isotropic and exhibits a $-5/3$-decay. Thus, for wave numbers smaller than κ_c, the turbulence is resolved, and for larger wave numbers, the turbulence is modeled. Since LES resolves the large-scale turbulence (note that the smallest scales resolved with LES are much smaller than those scales resolved with URANS as seen in Fig. 1.2), the size of the grid cells must not be larger than the size of the eddies to be resolved. The time step must be small enough to be able to resolve the frequency of the turbulent fluctuations that are to be resolved. Hence, a much finer grid and a smaller time step is needed for LES than for URANS simulations.

It is important to note that, since the range of the scales in the inertial subrange (region II in Fig. 1.1) increases with an increased Reynolds number, as explained in Section 1.1, the spatial and temporal resolution for LES also needs to be increased. This is the bottleneck of LES, it becomes computational very costly at high Reynolds numbers.

The largest eddies are the most energy-containing eddies that feed the cascade process with the turbulent kinetic energy extracted from the mean flow, as described in Section 1.1.

An accurate prediction of these large eddies is therefore essential to successfully simulate turbulent flows.

The largest turbulent scales in the energy spectrum are not isotropic. These turbulent scales are resolved with LES but are modeled based on mean flow properties with RANS. Moreover, the largest turbulent scales are strongly dependent on the source of origin. In the case of a geometrically induced flow separation, the eddy size is related to the size of the geometry causing the separation, e.g. the height of a backward facing step. For an attached boundary layer, the eddy size is proportional to the distance from the wall.

The more turbulent energy the modeling approach is able to resolve, the better ability it has to predict non-equilibrium flows and thus to adapt to a specific flow situation, as shown in Table 1.1.

Since RANS/URANS models are based on mean flow quantities, they need to be tuned to give accurate predictions for specific flow situations. This means essentially that RANS models are tuned to give a Reynolds stress tensor, based on mean flow quantities, that matches a specific flow situation. If the flow situation does not match the flow situation for which the RANS model is tuned, the model will most likely give a poor prediction of the flow. Typically, RANS models fail to give accurate predictions of non-equilibrium flows, such as massively separated flows where the large-scale turbulence is induced by a complex geometry.

Hence, taking the step from RANS to LES, the ability to accurately predict a wider range of flows, separated as well as attached flows, is much increased since LES resolves the large scale turbulence. On the other hand, the computational cost for applying LES to wall bounded flows at high Reynolds numbers is tremendously high as stated by e.g. Spalart [4, 5], due to the required spatial and temporal resolution, and will not be possible to use for industrial applications within the next decades.

To overcome the computational cost associated with LES simulations of wall bounded flows, many researchers have proposed turbulence modeling approaches in the recent decades where URANS and LES are combined, so called hybrid RANS-LES modeling[1](HRLM), see e.g. [6–12]. Generally, unsteady RANS is applied in the near-wall region and LES is applied in the off-wall region and in regions of separated flow. Thus, the strength of the RANS models to accurately predict attached flows at a low computational cost is combined with the strength of LES to predict the non-equilibrium separated flows in regions where the turbulent scales are much larger than in the near-wall region. Hybrid RANS-LES modeling is the focus in this thesis.

1.3 Hybrid RANS-LES modeling

Since the time that Spalart et al. [6] presented the Detached-Eddy Simulation (DES) concept in 1997, extensive research effort has been dedicated to the development of hybrid RANS-LES methods. Two main categories of HRLM have developed: non-zonal methods and zonal methods.

[1] Even though the turbulence modeling category is called hybrid RANS-LES, RANS in this context implicitly means unsteady RANS (URANS). However, hybrid RANS-LES is a well established nomenclature and will therefore be used throughout this thesis.

This section will give an introduction to hybrid RANS-LES modeling. First, non-zonal and zonal RANS-LES modeling approaches will be schematically described as well as typical shortcomings related to simulations where RANS and LES are combined. In the next subsections, an introduction is given to non-zonal methods and zonal methods including a brief review of different methods for applying turbulent fluctuation at LES inflow boundaries and RANS-LES interfaces. Finally, subgrid-scale modeling methods for grey-area mitigation are presented.

The most common and relatively mature hybrid RANS-LES methods use an explicit RANS-LES interface between the two modeling types, as in DES. However, during the past decade, a number of seamless hybrid RANS-LES methods have been proposed, for example Partially-Average Navier-Stokes (PANS, see e.g. [13]) and Partially-Integrated Transport Method (PITM, see e.g. [14]). These methods are seamless in the sense that no explicit RANS-LES interface is present to distinguish between RANS and LES modes. Both approaches are based on RANS models, which are modified to adapt to a scale resolving model, i.e. LES-like behaviour, where the turbulent fluctuations are strong and the grid resolution supports resolved turbulence. Otherwise the turbulent scales are modeled. Another example of turbulence-resolving modeling involving RANS and LES behaviour without any explicit interfaces is the Scale-Adaptive Simulation model (SAS, see e.g. [15]), which should be seen as an URANS model with scale-resolving capability. This thesis is concentrated to hybrid RANS-LES methods with an explicit RANS-LES interface.

In non-zonal methods, RANS is applied near solid walls in order to relax the resolution requirement in the near-wall region, compared to LES, and LES is applied in off-wall regions as well as in regions of separated flow, as shown in Fig 1.3. These methods automatically switch from RANS to LES based on a comparison between the local RANS and LES length scales. In general, the hybrid RANS-LES model simulates the flow using RANS if the local RANS length scale is smaller than the local LES length scale. Otherwise the flow is simulated using LES.

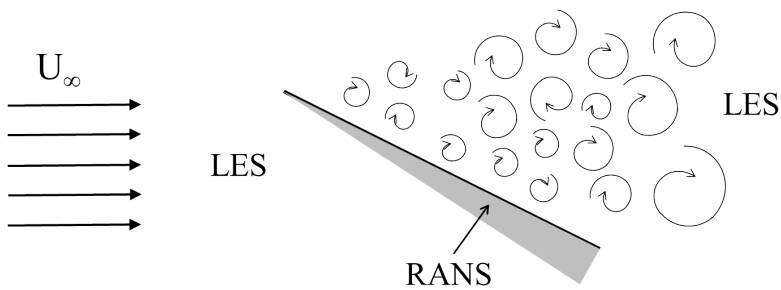

Figure 1.3: Schematic of non-zonal hybrid RANS-LES. Flat plate at high incidence. The attached boundary layer on the pressure side of the flat plate is modeled with RANS. The off-wall flow region and the separated flow is modeled with LES.

Even though hybrid RANS-LES simulations are computationally much less expensive than LES simulations, hybrid RANS-LES are order of magnitudes more costly compared

to RANS simulations, which are used as common praxis in the aeronautical industry today. With zonal hybrid RANS-LES approaches, where prescribed LES regions are embedded in a surrounding RANS region and applied only to specific regions of interest, e.g. regions of separated flow, it is possible to further reduce the computational costs compared to non-zonal HRLM. A schematic of a zonal approach, referred to as embedded LES, is presented in Fig. 1.4.

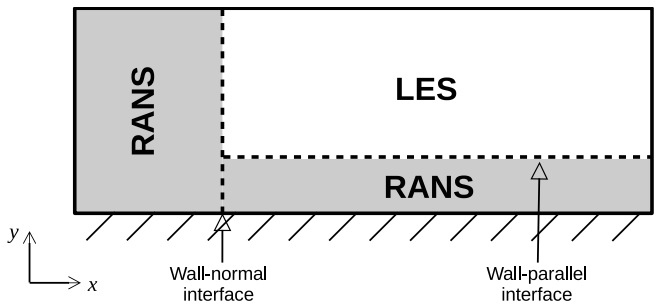

Figure 1.4: Schematic of RANS and LES regions in zonal hybrid RANS-LES (embedded LES) with wall-normal and wall-parallel RANS-LES interfaces indicated.

In non-zonal hybrid RANS-LES methods, the same basic transport equations for the turbulent quantities are often used in the RANS and LES regions. The turbulence-resolving LES mode of non-zonal hybrid RANS-LES methods is given by length-scale substitutions in the background RANS model, i.e. the RANS length scale is changed to a LES length scale based on the local grid size in suitable terms in the transport equation(s) for the turbulent quantities, see Section 1.3.2. This method is also used in zonal approaches. However, it is not unusual in zonal HRLM that different turbulence models are used in the RANS and LES regions, e.g. a $k-\omega$ turbulence model can be applied in the RANS region while an algebraic subgrid scale model is applied in the LES region.

It should be noted that, in the case the same basic transport equations are used in both RANS and LES regions, the turbulent quantities represent RANS levels in the RANS region and subgrid-scale levels in the LES region. For example, when a transport equation for turbulent kinetic energy is used in both regions, the turbulent kinetic energy represented in the RANS region is much larger than in the LES regions since only the subgrid-scale turbulent kinetic energy is modeled in LES.

1.3.1 Shortcomings in hybrid RANS-LES modeling

Across a RANS-to-LES interface, the hybrid RANS-LES model changes the modeling mode from RANS to LES. In other words, the modeling is switched from a non-turbulence-resolving method to a turbulence-resolving method.

Consider a RANS-LES interface where the main flow direction is across the interface from RANS to LES. Even though, the modeling mode is switched instantly across a single grid plane, the resolved turbulent stresses are not instantly fully developed. A certain

transition region downstream of the RANS-LES interface is needed for the LES simulated flow to establish fully developed resolved turbulent stresses. This transition region is the so-called "grey area", as mentioned by Spalart et al. when they proposed DES [6], and grey-area mitigation is thus ways to shorten the length needed to reach fully developed LES flow.

There are two reasons for the grey area to occur. First, in the RANS simulated flow, there are no or only weak natural instabilities that represent turbulent fluctuations and resolved turbulent stresses. These instabilities have to be developed in the LES region over a certain distance. Second, the turbulent viscosity from the RANS region, which is higher than in LES, is convected into the LES region across the interface. Hence, even though the RANS mode is switched over the interface to LES and the turbulent viscosity on the LES side becomes a modeled turbulent subgrid scale property, the turbulent viscosity is higher in the LES region near the interface than if the whole flow had been simulated using pure LES. The actual turbulent viscosity near the interface on the LES side of the interface is thus a heritage from the RANS region and its high level will act to damp the development of resolved turbulent stresses in the LES region.

It should be noted that, for flows where no or only weak natural fluctuations are present (e.g. attached boundary layer flows or free mixing layer flows), the grey area can be much more pronounced than in flows where strong natural fluctuations are present (e.g. large-scale separation flows) since the strong natural fluctuations trigger the equations to resolve the turbulence even though a high turbulent viscosity is convected from the RANS region.

In hybrid RANS-LES modeling, if the RANS mode is switched to LES inside the boundary layer, the grey area gives rise to the phenomenon known as log-layer mismatch. It means that the LES predicted velocity profile does not match the RANS predicted velocity profile due to the mismatch in the predicted turbulent stresses on each side of the RANS-LES interface. The mismatch is due to the rapid reduction of the turbulent viscosity across the RANS-LES interface and an under-prediction of the resolved stresses on the LES side of the interface. As a result of the log-layer mismatch, the skin friction is almost always under-predicted.

Different strategies are commonly used to remedy the grey area and the log-layer mismatch. Either turbulent fluctuations can be added at the inlet or onto the embedded wall-normal RANS-LES interface to overcome the grey-area caused by the absence of resolved turbulence in the RANS region. Methods to achieve a rapid reduction of the turbulent viscosity on the LES side of the interface can also be applied. Sometimes, a combination of the methods mentioned is used.

1.3.2 Formulation of hybrid RANS-LES methods

In the original DES model [6], which is based on the Spalart-Allmaras (SA) one-equation turbulence model, the destruction term in the transport equation for the turbulent viscosity is modified. In this term, the RANS length scale, namely the wall distance d, is present. When the LES mode is applied in DES, the wall distance is changed to the LES length scale based on the local grid size. Since the LES length scale is smaller than the RANS length scale in the LES region, the destruction term takes larger values. Hence,

the turbulent viscosity is reduced in the LES region and the momentum equations start to resolve the turbulence.

For the SA model, the destruction term is the only possible term where a length scale substitution can take place. However, for some turbulence models, alternative length scale substitutions are possible since the turbulent length scale can be present in more than one term in the background RANS model.

Yan et al. [16] explored different alternatives for modifications to the $k-\omega$ model by Wilcox [17]. Three different formulations were explored. First, the length scale substitution was applied only to the dissipation term in the equation for the turbulent kinetic energy. The second was as the first case, but, in addition, the turbulent viscosity was manipulated to explicitly include the length scale. Third, the length scale substitution was only applied to the turbulent viscosity.

It was highlighted in the study that there is possibility for the model, in its LES formulation, to reduce to a Smagorinsky model [18]. This means that, under local equilibrium conditions, i.e. when the production balances the dissipation, the turbulent viscosity can be expressed as $\nu_t = (C\Delta)^2 |S|$, where C is a constant (often called C_{DES} in DES type models), calibrated in Decaying Homogeneous Isotropic Turbulence (DHIT, see below), Δ is the filter width and $|S| = \left(2S_{ij}S_{ij}\right)^{0.5}$, where S_{ij} is the strain rate tensor.

In formulation one, where both k and ω equations are involved through the turbulent viscosity, local equilibrium must be satisfied in both equations simultaneously. This is not possible in RANS mode, but possible in LES mode due to the length scale substitution. This is shown in Section 3.1.2. This formulation is used in e.g. DES based on Menter's Shear-Stress-Transport $k-\omega$ model by Strelets [19]. This formulation is also used in the hybrid RANS-LES model developed in thesis.

Looking at the length scale substitution, where only the turbulent viscosity is involved (the third formulation), this formulation cannot re-create a Smagorinsky-like turbulent viscosity since production and dissipation/destruction do not balance in the k and ω equations simultaneously. For the second formulation, which reduces to a one-equation model for the subgrid-scale turbulent kinetic energy, it is straight forward to show that this model can be expressed in terms of a Smagorinsky turbulent viscosity. This formulation is used e.g. in X-LES by Kok et al. [8]. Even though all three formulations cannot reduce to a Smagorinsky-like turbulent viscosity, all three formulations give similar results for the computed test case, a NACA0012 profile at a 60-degree angle of attack.

Calibration of C_{DES}, which was done using DHIT, gave quite different results for the different formulations. The lowest value was achieved for the formulation only involving the dissipation term, and the highest value was given for the case where the length scale substitution was applied to both the dissipation term and the turbulent viscosity. The C_{DES} values were in the range of $0.70-0.95$. The authors interpreted the differences in C_{DES} values as an indication of the inherent dissipation of the turbulence model formulation, i.e. dissipation of turbulence. A low value of C_{DES} indicates a higher inherent dissipation compared to a formulation given a high C_{DES} value. Moreover, the authors linked the level of inherent dissipation to the term to which the length-scale modification has been applied. Applying the LES length scale only to the dissipation term in the k-equation, i.e. giving the lowest C_{DES} value and the highest inherent model dissipation, only the right part of the energy spectrum is affected, i.e. region III in

Fig. 1.1. Hence, this change affects the dissipation of turbulence from kinetic energy to heat through the molecular viscosity. As a secondary effect, the subgrid-scale turbulent kinetic energy is decreased, which in turn leads to a lower level of turbulent viscosity. In contrast, when both the destruction term in the k-equation and the turbulent viscosity are changed, the generation of the subgrid-scale turbulent kinetic energy is cut-off at the source since the turbulent viscosity is used to compute the turbulent stresses in the production term. This in turn, gives a more rapid effect on the reduction of turbulent viscosity compared to when only the dissipation term is changed. The authors concluded that the production and destruction terms can be described as having a strong and weak effect, respectively, on the turbulent dissipation.

It can be concluded from the work referred to that different length scale substitutions are possible when formulating the turbulence-resolving mode of hybrid RANS-LES models and that the models can be based on different underlying RANS models. Moreover, the reference work concludes that numerical tests, such as DHIT, are preferable to analytic derivations, which can give contradictory values of C_{DES}, in order to determine C_{DES}. Since the C_{DES} value is dependent on the discretization scheme used in the solver and the inherent numerical dissipation, its value is, to some extent, dependent on the code in which the hybrid RANS-LES model is implemented.

Non-zonal methods

The original DES formulation by Spalart et al. [6], based on the Spalart-Allmaras one equation model [20] (SA), switches from RANS to LES by taking the local minimum of the turbulent length scale of the SA model, the wall distance, d, the LES length scale that is used, and the maximum length of the local cell size, Δ_{max} (see Eq. 3.20). Later, Strelets [19] proposed DES based on Menter's SST $k-\omega$ model [21] (MSST), where the turbulent RANS length scale is based on k and ω, $l_{turb} = k^{1/2}/\left(\beta^{*}\omega\right)$. Contrary to DES based on the SA model, where $l_{RANS} = d$, the RANS length scale in DES based on the MSST model is based on k and ω, the RANS-LES switch in MSST-based DES is dependent on the flow field and not only the grid.

In the original DES formulation, the RANS-LES interface location is determined by the grid. With a drastic grid refinement in the streamwise and/or spanwise directions, e.g. to resolve a trailing edge separation on an aircraft wing or a shock-induced boundary layer separation, DES gives an undesirable switch from RANS to LES inside the boundary layer if $\Delta_{max} < \delta_{BL}$, where δ_{BL} is the boundary layer thickness. This leads to a reduction of the turbulent viscosity in the LES region, and often to a local under-prediction of the LES-resolved turbulent stresses, since the grid is not fine enough to support resolved velocity fluctuations and the near wall URANS region does not provide the LES region with any (or only weak) turbulent fluctuations. This modeling issue is commonly called Modeled Stress Depletion (MSD) [11], which in the worst case can lead to what is known as Grid Induced Separation (GIS) [22] due to the unphysical reduction of the turbulent stresses.

To prevent LES from penetrating into the boundary layer, and thus avoid MSD and GIS, Menter and Kuntz [22] proposed the use of a shielding function based on either of the F_1 or F_2 blending functions used in MSST. Later, Spalart et al. [11] proposed

Delayed DES (DDES) with a generalized shielding function, f_d, which does not rely on any specific background RANS model but only requires the use of a turbulent viscosity. Both methods effectively prevent LES content from entraining into the boundary layer and thus safely model the boundary layer with RANS.

In flows such as shallow flow separations, there is a strong coupling between the incoming boundary layer turbulence and the separation bubble. Resolved boundary layer turbulence is needed in hybrid RANS-LES simulations of such flows, at least in the outer part of the boundary layer, in order to accurately predict the flow. Hence, the LES flow content must be available in the incoming boundary layer, which implies that the model must switch from RANS to LES inside the boundary layer. With the aim of achieving such a capability, and to minimize the the log-layer mismatch in a non-zonal hybrid RANS-LES framework, Shur et al. [12] proposed Improved DDES (IDDES). Compared to DDES, IDDES has an additional wall-modeled LES (WMLES) capability, where the base RANS model acts as the wall model in WMLES mode. In IDDES, the WMLES mode is used if the boundary layer turbulence is strong, e.g. when it is generated by a synthetic turbulence generator and the grid is fine enough to support resolved boundary layer turbulence; otherwise, the DDES model is returned and the boundary layer is modeled in RANS mode.

As in DES, different background RANS models are also used in DDES and IDDES, where the most commonly used background RANS models are the SA and MSST models, especially for aeronautical applications. The DES variants have to be tuned depending on the background RANS model. For example, Gritskevich et al. [23] re-calibrated DDES and IDDES models to be based on MSST instead of SA. Gritskevich et al. [23] also proposed a simplified version of the IDDES model with negligible differences, when compared to the original formulation based on the SA model.

In addition to the DES-type models mentioned above, there are other similar non-zonal hybrid RANS-LES models, such as the eXtra-Large Eddy Simulation (X-LES) by Kok et al. [8] and the algebraic zero-equation hybrid RANS-LES model (HYB0) by Peng [10]. Contrary to the DES-type methods, where the destruction term in the SA model and the dissipation term in the k-equation in the MSST model are modified, both the dissipation term in the k-equation and the turbulent viscosity are modified in the TNT $k-\omega$ model [24] used as the base RANS model in X-LES. The HYB0 model is designed as a wall-modeled LES model whereas DES and DDES are designed to model the entire boundary layer in RANS mode.

Zonal methods and inflow/interface turbulent fluctuations

As mentioned in Section 1.3, the aim of zonal RANS-LES/embedded LES approaches is to concentrate the turbulence resolving methods to regions of interest, e.g. regions of separated flow, in order to reduce the computational cost compared to LES and non-zonal hybrid RANS-LES simulations. There are two main strategies for embedded LES. Using the same nomenclature as in Shur et al. [25], embedded LES approaches can be categorized as two-stage semi-coupled or one-stage fully coupled.

Semi-coupled approaches use a precursor RANS simulation in order to provide the boundary conditions for the subsequent turbulence-resolving simulation. Since the two

simulations are not performed simultaneously, this approach is not suitable for flows where the flow downstream of a wall-normal RANS-to-LES interface strongly affects the upstream RANS flow. With fully coupled approaches, the RANS and the LES regions are computed simultaneously so that information between the two regions can be exchanged.

Due to the absence of resolved turbulence in the RANS region, addition of turbulent fluctuations is often needed at the wall-normal LES inflow boundary to mitigate the grey area. A common and versatile approach is to use synthetic turbulent fluctuations, i.e. artificial turbulent fluctuations generated to mimic the physical turbulent fluctuations of the actual flow. Another approach is to recycle turbulent fluctuations from a downstream location in the flow, rescale the fluctuations and add them at the upstream wall-normal RANS-LES interface. A third approach is to use precursor simulations or data bases, based on e.g. DNS or LES, and add these (rescaled) fluctuations at the RANS-LES interface.

The latter method is limited since DNS and LES are restricted to low Reynolds-number flows due to the high computational cost associated with these simulation techniques. Scaling of turbulent fluctuations for a wide Reynolds number range is non-trivial and probably not possible for high Reynolds numbers. Hence, the practical use of precursor-based methods for industry applications are limited.

Quéméré and Sagaut [26] successfully demonstrated fully coupled zonal RANS-LES simulations of flow over a flat plate with a blunt trailing edge to efficiently compute aeroacoustic sources. The trailing edge separation region, simulated as a three-dimensional region with LES, was coupled to the surrounding two-dimensional RANS region, represented by the upstream flat plate boundary layer and the freestream flow. The turbulent inlet fluctuations to the LES region, applied at a wall-normal RANS-LES interface, were taken from an auxiliary LES computation.

On the basis of the idea of combining two-dimensional RANS and three-dimensional LES, Terracol [27] also demonstrated trailing edge separation flow for aeroacoustic purposes. He applied the proposed approach to flow over a flat plate with a blunt trailing edge and a NACA0012 airfoil. Two different approaches for applying inlet turbulent fluctuations to the LES region, which was limited to the trailing edge separation region, were compared: a recycling method and a method with synthetic turbulent fluctuations. Both methods applied the turbulent fluctuations at wall-normal RANS-LES interfces. It was concluded that both methods gave a good reproduction of the turbulent structures seen in the reference LES (where the entire domain was simulated with LES without any inclusion of RANS regions) in the separated trailing edge region. However, the frequency at which the recycling was made was clearly represented as peaks in the pressure spectrum in the trailing edge wake, leading to the conclusion that the methodology using the synthetic inlet turbulent fluctuations was better suited for aeroacoustic applications.

Fully coupled zonal RANS-LES simulations of a three-dimensional highly curved inlet duct were made by Mary [28] using an overlapping grid technique to find an efficient simulation method for predicting strongly separated inlet flows. To reduce the grid size, only half of the channel leading into the curved duct was simulated using a symmetry condition. Inlet fluctuations to the LES region were taken from a database. The inlet fluctuations were rescaled to fit turbulent time and length scales for the simulated flow. It was concluded that the full domain must be simulated (i.e. no symmetry plane can

be used) and that it was not possible to use generalized turbulent fluctuations from the database that was employed to achieve accurate results. Moreover, dominant low-frequency fluctuations in the flow needed a very large statistical dataset: i.e. data representing a long physical time period, typically in the order of seconds, to accurately represent the flow.

Deck successfully demonstrated Zonal Detached-Eddy Simulation (ZDES) for the flow over a multi-element airfoil [9, 29]. A combination of RANS and DES was used in attached and separated flow regions, respectively. The predicted turbulence-resolving flow is remarkably good, but no turbulent fluctuations were added at the embedded RANS-DES interfaces. It should be noted that the DES used by Deck is slightly modified compared to the original DES [6]. The LES length scale Δ_{vol} (or Δ_{Ω} in later version [29, 30]) is used instead of Δ_{max}. Furthermore, Deck switched off the low-Reynolds-number damping functions, that are present in the SA-RANS model [20], in LES mode.

Zhang et al. [31] demonstrated fully coupled zonal RANS-LES simulations of a wing-flap airfoil configuration, where the attached flow was simulated with two-dimensional RANS and the separated cove and trailing edge flow were simulated with LES. At the inlet boundaries to the LES-simulated flow regions, forcing was used. Zhang et al. [31] concluded that, by using a zonal partitioning of the multi-element airfoil, they reduced the computational cost by approximately 50% compared to a full LES computation. However, the LES computation referred to was made on a relatively coarse grid and a narrow domain in the spanwise direction.

A wide range of flows simulated with a fully coupled zonal RANS-IDDES [12] approach is given in Shur et al. [25]. Examples of simulated flows are: plane mixing-layer flow, trailing edge flow and flow over a wall-mounted hump. Two methods for synthetic turbulence generators are outlined, one for aerodynamic purposes and one for aeroacoustic purposes. Both methods applies the synthetic turbulent fluctuations at wall-normal RANS-LES interfaces. Moreover, both methods have the aim of reproducing typical near-wall turbulent structures for application to WMLES and with the capability to rapidly recover wall-bounded flows from a fully developed RANS state to a fully developed turbulence-resolving state. The latter method, adapted for acoustic applications, is designed to suppress the spurious noise generated by the synthetic turbulence generator by inserting an internal damping layer in the LES region downstream of the wall-normal RANS-LES interface.

Semi-coupled zonal RANS-LES simulations of the wall-mounted hump flow have also been demonstrated with good results by Davidson and Peng [32]. In their work, boundary condition data for the subsequent LES were taken from an MSST precursor RANS simulation. The LES was based on PANS [33] and anisotropic synthetic turbulent fluctuations were applied at the wall-normal LES inlet boundary [34, 35].

In the above mentioned zonal approaches, the mean flow was approximately orthogonal to the RANS-to-LES interface. However, for a wall-parallel interface, where the mean flow is almost parallel to the RANS-LES interface, the grey area issue, often lead to the log-layer mismatch, which is also important. This was advocated by e.g. Davidson and Peng [7] and Nikitin et al. [36] (using DES as a wall-modeled LES) in simulations of fully developed channel flow.

To reduce the log-layer mismatch in fully developed channel flow, Davidson and

Dahlström [37] used forcing at the wall-parallel RANS-LES interfaces to add turbulent fluctuations. The turbulent fluctuations were taken from a precursor DNS of a generic boundary layer and rescaled to match the simulated flow conditions. The work by Davidson and Billson [35] presents fully developed channel flow simulations where synthetic turbulent fluctuations were added at the wall-parallel RANS-LES interfaces. In both these works, the log-layer mismatch was substantially reduced, even though very coarse grids were used in the LES region of the simulated channel flows.

Additional turbulent energy is introduced by superimposing synthetic turbulent fluctuations to the RANS mean flow field at the RANS-to-LES interface. Hence, a transfer of modeled turbulent kinetic energy to resolved turbulent kinetic energy (i.e. a reduction of the modeled turbulent kinetic energy) must be forced to avoid an excess of turbulent kinetic energy (and turbulent viscosity) on the LES side of the interface.

Hamba [38] used filtered DNS data to explore the commutation error, due to the non-commutivity of the spatial derivative and the filter applied in RANS and LES, at the RANS-LES interface. He argued that the commutation error can be large across the RANS-LES interface and thus must be considered. Girimaji and Wallin [39] applied Hamba's theory to PANS simulations of Decaying Homogeneous Isotropic Turbulence (DHIT). They showed that the proposed commutation terms can be used to give the required transfer of modeled-to-resolved/resolved-to-modeled turbulent kinetic energy without any use of empirical constants.

The commutation terms proposed by Hamba were further explored by Davidson [40, 41] in combination with synthetic turbulent fluctuations at wall-normal interfaces in hybrid RANS-LES simulations in order to reduce the RANS turbulent viscosity to SGS levels and to promote a rapid growth of the turbulence-resolving LES flow.

Subgrid scale modeling for grey-area mitigation

Most commonly, hybrid RANS-LES methods reduces to a Smagorinsky-like m odel in LES mode. Hence, the subgrid scale turbulent viscosity is proportional to the square of the LES filter width, $\nu_t \propto \Delta^2 |S|$. An excess of the subgrid scale turbulent viscosity can be avoided by adapting the filter width to the local flow situation, which is advantageous for a rapid development of the resolved turbulent fluctuations.

In SA-based DES simulations of flow over a flat plate at a high incidence made by Breuer et al. [42], it was concluded that the formation of the resolved turbulence in the free shear layer, emanating from the leading edge of the flat plate, was better predicted using Δ_{vol} (see Eq. 3.21) than with Δ_{max} (see Eq. 3.20), due to the lower level of the subgrid-scale turbulent viscosity produced with Δ_{vol}.

On the basis of stronger physical arguments for the behaviour of free shear layers, Chauvet et al. [30] proposed a LES length scale involving the local vorticity field, Δ_Ω (see Eq. 3.22), where the filter width is expressed as the square root of the plane perpendicular to the spin axis of the local vorticity. The formulation of this length scale was later generalized to unstructured grids by Deck [29]. Improved predictions have been made with this LES length scale, using hybrid RANS-LES simulations of e.g. a controlled propulsive jet [30] and plane free shear layers [29].

The vorticity-based LES length scale was further developed by Mockett et al. [43] in

order to limit the influence of the smallest edge of the local cell, which is dominant in the original formulation [29, 30]. Further, Shur et al. [44] proposed a flow sensor to detect early shear layers in order to design a universal LES length scale for attached, separated and free shear-layer flows. When a shear layer flow is detected, the vorticity-based LES length scale by Mockett et al. [43] is used; otherwise, the original length scale of e.g. DDES is applied.

Moreover, Mockett et al. [43] combined their vorticity based LES length scale with alternative SGS models, which better adapts to the local flow field as compared to the commonly used Smagorinsky model, resulting in a reduced RANS-to-LES transition region and an improved prediction of a free shear-layer flow. With a stochastic subgrid-scale model and a high-pass filtered subgrid-scale model, Kok and van der Ven [45] showed that it is possible to accelerate the transition from RANS to LES in a plane shear layer flow and in a vortex breakdown flow over a delta wing with a sharp leading edge.

Peng et al. [46, 47] introduced a velocity-gradient-based term (i.e. the Leonard term) in the SGS modeling in conjunction to conventional eddy-viscosity based models. The Leonard term plays a role in the instantaneous energy backscatter, and thus enables to enhance the resolved turbulent fluctuations in the LES region.

1.4 Motivation and aeronautical industry needs

Flows around aircrafts are characterized by high Reynolds numbers and separated flow, e.g. at maneuvering conditions or at landing conditions when landing gears are extracted and high-lift devices are deployed. Further, for transonic and supersonic aircraft, shock/boundary-layer interaction phenomena can be present, which can cause flow induced noise and structure fatigue as well as affect the aircraft performance. Many of these phenomena are unsteady and are characterized by large scale turbulence.

With increased computational resources available for industry, Computational Fluid Dynamics (CFD) and RANS techniques serve today as the main tool for design and analysis of aircraft aerodynamics. Moreover, CFD is commonly used in multi-disciplinary applications such as fluid-structure interaction and aero acoustics. However, as stated in Section 1.2 above, RANS methods perform well for attached and mildly separated flows. Hence, applying RANS methods to massively separated flows, as those described above, often results in poor flow predictions.

Since most of the flow simulations in the aeronautical industry today are performed using RANS modeling techniques, there are many flight conditions that are poorly predicted or not possible to simulate with industry standard techniques. However, due to the high costs associated with wind tunnel testing and full scale flight tests, high fidelity CFD methods, such as LES based turbulence modeling approaches and high order methods, are good candidates for reducing these costs.

Pure LES of full scale aircrafts are not affordable today and will not be affordable for many decades ahead [4, 5]. High order methods have been demonstrated in complex turbulent flows, but there are still bottlenecks associated with these methods that must be resolved in order to be able to use them as industry standard tools. Owing to the much reduced resolution requirement in space and time for hybrid RANS-LES methods

as compared to LES and the fact that the computer capacity will likely not develop as rapidly as it has done during the last decades, hybrid RANS-LES modeling seem to be the best candidate today for simulating complex industrial turbulent flows at high Reynolds numbers at an affordable computational cost [5].

This thesis is motivated by the needs for improved simulation accuracy and increased computational efficiency for the complex turbulent flows present in aeronautical applications. Using hybrid RANS-LES modeling techniques thus fulfills these requirements. Even though hybrid RANS-LES simulations have been used for the past two decades, the interface connecting the RANS and the LES simulated flows is still a challenging task that needs special attention in order to increase simulation robustness and accuracy in industrial applications. The focus of this thesis is therefore RANS-LES interface methodologies and how hybrid RANS-LES models can be adapted to give improved turbulence-resolving capability in the RANS-LES interface region for increased accuracy and robustness.

2 Governing equations and numerical methods

This chapter introduces the governing equations for turbulent flows, the filtered Navier-Stokes equations. As mentioned in the introduction, it is today not affordable to conduct DNS for flows of engineering interest. The equations need to be filtered in order to reduce the spatial and temporal resolution. The filtered Navier-Stokes equations are presented for incompressible and compressible flows and the CFD solvers used in this thesis, to numerically solve the filtered Navier-Stokes equations, are briefly described.

In hybrid RANS-LES simulations, RANS and LES are combined. The RANS equations are time-averaged (Eq. (2.1)) whereas a spatial filter (Eq. (2.2)) is used in the LES equations. That means that two different filtering approaches are combined in the same simulation. Hybrid RANS-LES is seen as a pragmatic, but well established, approach used to solve the problem with the high computational cost associated with LES of wall-bounded flow at high Reynolds numbers.

The two filter types, time-averaging and spatial filtering, can be interpreted in hybrid RANS-LES such that different sized spatial filters, Δ, are applied in order to model different ranges of turbulent scales, i.e. differently sized turbulent eddies. Hence, RANS should represent a large sized spatial filter (much larger than the spatial filter applied in LES) that models a much wider range of turbulent scales than LES, ranging from the largest turbulent scales, represented by the RANS length scale, to the smallest turbulent scales. The filter size in LES is much smaller, and thus only the smaller turbulent scales are modeled. With this interpretation of the different filter types, the URANS modeled flow in hybrid RANS-LES simulations can be referred to as Very Large Eddy Simulation (VLES), as in Davidson and Peng [7].

Using the analogy with different sized spatial filters for RANS and LES, the filter size is reflected, for eddy-viscosity-based modeling, in the level of the turbulent viscosity (the larger the turbulent length scale, the higher the level of turbulent viscosity), which is the only quantity referring to the modeled turbulence that is fed into the Navier-Stokes equations. Navier-Stokes equations, either in RANS mode or in LES mode, only "feel" the turbulent viscosity, which can be large or small depending on the filter width applied, resulting in a LES resolving flow or a RANS simulated flow. It is important to note that, in the RANS region, e.g. close to the wall, the turbulent viscosity is lower in hybrid RANS-LES simulations than in pure RANS, see e.g. Davidson [40]. Due to the lower RANS turbulent viscosity in hybrid RANS-LES, the very large scale turbulence is resolved in the near-wall region unlike pure (U)RANS. Hence, it seems reasonable to view the RANS part of hybrid RANS-LES as a VLES.

From now on, $(\bar{\cdot})$ means time-averaging when RANS is applied and spatial filtering when LES is used. The time-averaging used to derive the RANS equations can for an arbitrary quantity Φ be expressed as

$$\overline{\Phi} = \lim_{T\to\infty} \frac{1}{T} \int_{-T/2}^{T/2} \Phi dt, \qquad \Phi = \overline{\Phi} + \Phi' \tag{2.1}$$

where Φ' denotes the fluctuating part of Φ. Spatial filtering of the quantity Φ, here using a 1D filter for simplicity, reads

$$\overline{\Phi}(x,t) = \frac{1}{\Delta x}\int_{x-0.5\Delta x}^{x+0.5\Delta x} \Phi(\xi,t)\, d\xi, \qquad \Phi = \overline{\Phi} + \Phi'' \tag{2.2}$$

where Φ'' denotes the modeled part of Φ. Moreover, since finite volume discretization is used in this thesis, the spatial filter is represented by the local control volumes based on the computational grid, so-called implicit filtering.

Using eddy-viscosity models, e.g. the PDH-LRN model [48] described in Section 3 below, the subgrid scale turbulent stresses are modeled using Boussinesq's assumption

$$-\rho\overline{u_i'u_j'} = \mu_t\left(\frac{\partial\overline{u}_i}{\partial x_j} + \frac{\partial\overline{u}_j}{\partial x_i} - \frac{2}{3}\frac{\partial\overline{u}_k}{\partial x_k}\delta_{ij}\right) - \frac{2}{3}\rho k\delta_{ij} \tag{2.3}$$

where $\mu_t = \rho\nu_t$ is the turbulent viscosity given by the turbulence model, ρ is the density and k is the turbulent kinetic energy. Note that for incompressible flow, $\partial\overline{u}_k/\partial x_k = 0$ due to the continuity. In hybrid RANS-LES, μ_t, represents either a RANS or a SGS turbulent viscosity depending on the modeling mode used.

2.1 Incompressible flows

The instantaneous incompressible filtered Navier-Stokes equations used in the flow simulations included in this thesis read

$$\frac{\partial\overline{u}_i}{\partial x_i} = 0 \tag{2.4}$$

$$\frac{\partial\overline{u}_i}{\partial t} + \frac{\partial\left(\overline{u}_i\overline{u}_j\right)}{\partial x_j} = -\frac{1}{\rho}\frac{\partial\overline{p}}{\partial x_i} + \frac{\partial}{\partial x_j}\left(\nu\frac{\partial\overline{u}_i}{\partial x_j} - \tau_{ij}\right) \tag{2.5}$$

where $\tau_{ij} = \overline{u_iu_j} - \overline{u}_i\overline{u}_j$ denotes the subgrid scale turbulent stresses, which need to be modeled. In Eq. (2.4) and (2.5), constant density and viscosity are assumed. The turbulent stresses are computed using Boussinesq's assumption

$$\tau_{ij} = \overline{u_i'u_j'} = -2\nu_t\overline{S}_{ij} \tag{2.6}$$

where ν_t is the turbulent viscosity, k is the turbulent kinetic energy and $\overline{S}_{ij} = 1/2\left(\partial\overline{u}_i/\partial x_j + \partial\overline{u}_j/\partial x_i\right)$ is the strain rate tensor. In the flow solver used, see below, the term involving k in Eq. (2.3) is included in the pressure. Moreover, the turbulent cross-diffusion term $\partial/\partial x_j\left(\nu_t\partial\overline{u}_j/\partial x_i\right)$ is omitted due to stability problems in RANS.

The single-block structured in-house solver CALC-LES was used to solve the incompressible Navier-Stokes equations presented in Eq. (2.4) and (2.5). The solver offers different spatial discretization schemes of first and second order: central differencing, van Leer and a hybrid scheme. Different schemes were applied depending on the application. The discretization schemes used in the simulations are specified in the papers appended to this thesis. The time advancement is made with a second order Crank-Nicolson

scheme. An implicit, fractional-step technique with an efficient multigrid Poisson solver [49] was used on a non-staggered grid arrangement. For a more detailed description of the numerical procedure, see Davidson and Peng [7].

2.2 Compressible flows

In addition to the filters given in Eq. (2.4) and (2.5), it is convenient to introduce Favré-averaging to the Navier-Stokes equations for compressible flow in order to avoid modeling of extra unknown terms. The Favré average is a density weighted average which, defined for an arbitrary quantity Φ, reads

$$\widetilde{\Phi} = \frac{\overline{\Phi\rho}}{\overline{\rho}}, \qquad \Phi = \widetilde{\Phi} + \Phi'' \tag{2.7}$$

where Φ'' is the subgrid scale part of Φ. The Favré average is applied to the velocities, the total energy and the temperature.

The Favré-averaged compressible Navier-Stokes equations with modeling assumptions, used in the compressible flow simulations included in this thesis, is outlined below. The continuity, momentum and energy equations, with $\widetilde{(\cdot)}$ denoting Favré-averaging, read

$$\frac{\partial\overline{\rho}}{\partial t} + \frac{\partial\left(\overline{\rho}\widetilde{u}_i\right)}{\partial x_i} = 0 \tag{2.8}$$

$$\frac{\partial\left(\overline{\rho}\widetilde{u}_i\right)}{\partial t} + \frac{\partial\left(\overline{\rho}\widetilde{u}_i\widetilde{u}_j\right)}{\partial x_j} = -\frac{\partial\overline{p}}{\partial x_i} - \frac{\partial\tau_{ij}}{\partial x_j} \tag{2.9}$$

$$\frac{\partial\left(\overline{\rho}\widetilde{e}_0\right)}{\partial t} + \frac{\partial\left(\overline{\rho}\widetilde{e}_0\widetilde{u}_j\right)}{\partial x_j} = -\frac{\partial\overline{p}\widetilde{u}_j}{\partial x_j} + \frac{\partial}{\partial x_j}\left[\left(\mu + \frac{\mu_t}{\sigma_k}\right)\frac{\partial k}{\partial x_j} - q_j - \widetilde{u}_i\tau_{ij}\right] \tag{2.10}$$

where $\overline{p}$ is the static pressure, μ is the molecular dynamic viscosity computed using Sutherland's law and μ_t is the turbulent dynamic viscosity given by the turbulence model. The stresses are computed using Boussinesq's assumption

$$\tau_{ij} = -\left(\mu + \mu_t\right)\left(\frac{\partial\widetilde{u}_i}{\partial x_j} + \frac{\partial\widetilde{u}_j}{\partial x_i} - \frac{2}{3}\frac{\partial\widetilde{u}_k}{\partial x_k}\delta_{ij}\right) + \frac{2}{3}\overline{\rho}k\delta_{ij} \tag{2.11}$$

where k is the modeled turbulent kinetic energy defined as

$$k = \frac{1}{2}\widetilde{u_k''u_k''} \tag{2.12}$$

The static pressure $\overline{p} = (\gamma - 1)\,\overline{\rho}\left(\widetilde{e}_0 - \frac{1}{2}\widetilde{u}_k\widetilde{u}_k - k\right)$. The total energy is computed as

$$\widetilde{e}_0 = \widetilde{e} + \frac{1}{2}\widetilde{u}_k\widetilde{u}_k + k \tag{2.13}$$

where $\tilde{e}$ is the internal energy. Fourier's heat law is applied to compute the the heat fluxes, which gives

$$q_j = -(\kappa + \kappa_t)\frac{\partial \tilde{T}}{\partial x_j}, \qquad \kappa = C_p\frac{\mu}{Pr}, \qquad \kappa_t = C_p\frac{\mu_t}{Pr_t} \tag{2.14}$$

where κ and κ_t are the viscous and turbulent thermal conductivities, respectively, Pr and Pr_t are the viscous and turbulent Prandtl numbers, respectively, and C_p is the specific heat coefficient for a constant pressure process.

The unstructured flow solver Edge [50] was used to solve the compressible Navier-Stokes equations given above. For steady state problems, Edge uses an explicit three-stage Runge-Kutta scheme with agglomerated multi-grid and residual smoothing for convergence acceleration. A dual time-stepping approach is applied for unsteady simulations, combining the Runge-Kutta method with an implicit second-order scheme for physical time advancement. A second order central differentiating scheme has been used for the spatial discretization of the momentum equations and the turbulent transport equations.

3 Development of a zonal hybrid RANS-LES approach

The chapter presents the zonal RANS-LES model developed during this thesis work. It also describes, the RANS-LES interface methodologies that are used to reduce the log-layer mismatch and to mitigate the grey area when the model is switched from RANS to LES.

3.1 Hybridization of the PDH-LRN $k-\omega$ model

In this section the choice of the background RANS model for the proposed hybrid RANS-LES model is motivated. The background RANS model is presented and briefly described. The LES mode of the proposed model is formulated, and this is followed by a résumé of the LES length scales used with the proposed hybrid RANS-LES model in this thesis.

3.1.1 The background RANS model

Paper A reported simulations of transonic flow in a rectangular duct. The reported flow case involves shock/boundary-layer interaction (SBLI). Local recirculation bubbles are present in the corners of the rectangular duct where the shock is located. The paper made a comparison of several models, including RANS models and turbulence-resolving approaches. Most of the models had difficulty to accurately predicting the onset of the separation bubble caused by the shock, due to an inaccurately predicted incoming boundary layer. It was concluded that the near-wall modeling is essential for the studied flow case, due to the SBLI phenomenon, as well as for the prediction of local recirculation bubbles. Among the models employed in the study, none of the hybrid RANS-LES models used gave an accurate prediction of the flow. The Low-Reynolds-Number $k-\omega$ RANS model by Peng et al. [48] (PDH-LRN), on the other hand, performed well and was able to appropriately represent the flow field.

In hybrid RANS-LES modeling, the PDH-LRN model is thus selected as the background RANS model with the aim to improve the prediction of the reported flow case using a hybrid RANS-LES modeling approach. Moreover, one of the purposes of this thesis is to find a suitable RANS base model for flows where local and shallow separation occurs, typically flows present in inlets of fighter jets. The fact that the PDH-LRN model is designed and intended for recirculating flows is desirable for it to be used as a background RANS model for further exploration in hybrid RANS-LES computations.

The PDH-LRN model is developed from Wilcox's low-Reynolds-number $k-\omega$ model [51]. Along with a re-calibration of model constants and damping functions, compared to Wilcox's model, an additional turbulent cross-diffusion term was added in the ω-equation in the PDH-LRN model. Contrary to Menter's BSL and SST models [21], where the cross-diffusion term is activated in the off-wall region (the region where $k-\epsilon$ is applied), the cross-diffusion term in PDH-LRN is active in both the near-wall and off-wall regions.

The transport equations and the turbulent viscosity for the PDH-LRN $k-\omega$ model read

$$\frac{D\rho k}{Dt} = \tau_{ij}\frac{\partial u_i}{\partial x_j} - D^k + \frac{\partial}{\partial x_j}\left[\left(\mu + \frac{\mu_t}{\sigma_k}\right)\frac{\partial k}{\partial x_j}\right] \tag{3.1}$$

$$\begin{aligned}\frac{D\rho\omega}{Dt} &= C_{\omega_1} f_\omega \frac{\omega}{k}\tau_{ij}\frac{\partial u_i}{\partial x_j} - C_{\omega 2}\rho\omega^2 \\ &+ \frac{\partial}{\partial x_j}\left[\left(\mu + \frac{\mu_t}{\sigma_\omega}\right)\frac{\partial \omega}{\partial x_j}\right] + C_\omega \frac{\mu_t}{k}\frac{\partial k}{\partial x_j}\frac{\partial \omega}{\partial x_j}\end{aligned} \tag{3.2}$$

$$\mu_t = C_\mu f_\mu \frac{\rho k}{\omega} \tag{3.3}$$

In Eqs. (3.1) and (3.2), D/Dt on the left hand side of the transport equations is the material derivative; $D/Dt = \partial/\partial t + u_i \partial/\partial x_i$. It should be noted that, close to the wall, the derivatives of k and ω are often of opposite signs, giving that the cross-diffusion term sometimes acts as a sink term in the ω-equation. In the near-wall region, k is thus increased due to the reduction of ω and, in turn, increased turbulent viscosity is achieved.

The functions f_k, f_ω and f_μ (see Eqs. (3.4)-(3.6)) are the low-Reynolds-number damping functions used in the k and ω equations and in the expression for the turbulent viscosity. These functions use the turbulent Reynolds number (see Eq. (3.7)) as the governing parameter, which is seen as an advantage compared to any wall distance related quantity. Wall distance based quantities can be ambiguous to define for complex geometries, whereas the turbulent Reynolds number is well defined since no geometrical properties are involved. On the other hand, in a hybrid RANS-LES perspective, the wall distance has been shown to be a suitable parameter to involve in the formulation of the LES length scale [12]. Thus, in turbulence-resolving simulations, it might be necessary to include the wall distance. The low-Reynolds-number damping functions used in the PDH-LRN model reads

$$f_k = 1 - 0.722 \cdot \exp\left[-\left(\frac{R_t}{10}\right)^4\right] \tag{3.4}$$

$$f_\omega = 1 + 4.3 \cdot \exp\left[-\left(\frac{R_t}{1.5}\right)^{1/2}\right] \tag{3.5}$$

$$\begin{aligned}f_\mu = 0.025 &+ \left\{1 - \exp\left[-\left(\frac{R_t}{10}\right)^{3/4}\right]\right\} \\ &\left\{0.975 + \frac{0.001}{R_t}\cdot\exp\left[-\left(\frac{R_t}{200}\right)^2\right]\right\}.\end{aligned} \tag{3.6}$$

The turbulent Reynolds number is defined as

$$R_t = \frac{k}{\nu\omega} \tag{3.7}$$

and the closure constants for the PDH-LRN model are

$$\sigma_k = 0.8 \quad \sigma_w = 1.35 \quad C_\mu = 1.0 \quad C_k = 0.09$$
$$C_{\omega 1} = 0.42 \quad C_{\omega 2} = 0.075 \quad C_\omega = 0.75$$

3.1.2 The LES mode

As highlighted in Yan et al. [16] and in Section 1.3.2, different alternative length scale substitutions can be possible in the background RANS model in order to achieve a hybrid RANS-LES model. In the PDH-LRN model, all three possibilities described in Yan et al. [16] can be used. Alternative one is chosen in the hybridization of the PDH-LRN model, i.e. only the dissipation term in the transport equation for the turbulent kinetic energy equation is modified. The ω-equation is left untouched, as is the expression for the turbulent viscosity. Hence, both k and ω will be used to compute the subgrid scale turbulent viscosity and are thus involved in the LES mode of the PDH-LRN based model. This is the same strategy as is used for DES based on MSST by Strelets [19].

The dissipation term in the PDH-LRN model is rewritten to explicitly include the turbulent length scale. The hybridization of the PDH-LRN model is made by changing the turbulent length scale depending on whether the flow should be modeled in RANS mode or LES mode. The dissipation term of the PDH-LRN model with the turbulent length scale reads

$$D^k = C_k f_k \rho k \omega = \rho f_k \frac{k^{3/2}}{l_{turb}} \tag{3.8}$$

The turbulent length scale is chosen according to the modeling mode, i.e. $l_{turb} = l_{RANS}$ or $l_{turb} = l_{LES}$ for RANS and LES, respectively.

$$l_{RANS} = \frac{k^{1/2}}{C_k \omega} \tag{3.9}$$

$$l_{LES} = \Psi_{PDH} C_{LES} \Delta \tag{3.10}$$

With $l_{turb} = l_{RANS}$, the original PDH-LRN model is returned. When $l_{turb} = \Psi_{PDH} C_{LES} \Delta$, the LES mode of the proposed hybrid RANS-LES model is achieved. Δ is the LES length scale and $C_{LES} = 0.70$ was calibrated using decaying homogeneous isotropic turbulence (DHIT). These results are presented in more detail in paper B. Different formulations of the LES length scale Δ have been evaluated in this thesis in an attempt to reduce the log-layer mismatch and mitigate the grey area. Since the PDH-LRN model uses low-Reynolds-number damping functions, the correction function, Ψ_{PDH}, is added to the LES formulation, as recommended by Spalart et al. [11]. Modeling constants and damping functions in the proposed hybrid RANS-LES model are unchanged as compared to the PDH-LRN model [48].

Contrary to RANS modeling where all turbulent scales are modeled, only the subgrid scale turbulence is modeled in LES. Thus, the local turbulent Reynolds numbers in LES

may become much lower as compared to RANS, which can activate the low-Reynolds-number damping functions. Since the amount of modeled subgrid scale turbulence is dependent on the grid resolution, the local turbulent Reynolds number and the turbulent viscosity are dependent of the grid resolution as well. The amount of damping achieved by the damping functions is hence dependent on the grid resolution, a dependency which should be avoided. The purpose of the correction function, Ψ_{PDH}, is to eliminate the low-Reynolds-number damping made by the damping functions in the LES region and to keep them in the RANS region. At local equilibrium, the introduction of Ψ_{PDH} is equivalent to deactivating the damping functions in LES mode. However, the damping functions should be used when RANS is applied. Through the introduction of the correction function in the LES length scale, the same set of model constants/equations can thus be used in both the RANS and LES regions. The correction function will now be derived for the PDH-LRN model in accordance with the work of Mockett [52].

A generalized form of the Smagorinsky turbulent viscosity can be formulated for the PDH-LRN model using the function A_{PDH} and the correction function Ψ_{PDH}.

$$\nu_t = A_{PDH} \left(\Psi_{PDH} C_{LES} \Delta\right)^2 S \tag{3.11}$$

To return the original formulation of the Smagorinsky turbulent viscosity, the correction function should cancel the low-Reynolds-number dependency of A_{PDH}, i.e. $A_{PDH}\Psi_{PDH}^2 =$ const. Assume that the proposed model is in LES mode, the simulated flow is away from the wall and that the turbulent transport equations are in local equilibrium, i.e. when production and dissipation/destruction are in balance in the k and ω equations. Note that, in RANS mode, the k and ω equations cannot be in local equilibrium simultaneously. However, due to the formulation of the dissipation term in the k-equation in LES mode, local equilibrium can be fulfilled away from the wall for the k and the ω equations, as seen in Fig. 3.1. The budgets seen in Fig. 3.1 are computed using the LES mode of the proposed hybrid RANS-LES model with the LES length scale Δ_{dw} (see Eq. (3.23)) in fully developed channel flow at $Re_\tau = 950$ [53].

The k and ω equations in LES mode at local equilibrium reads

$$\nu_t S^2 = f_k \frac{k^{3/2}}{\Psi_{PDH} C_{LES} \Delta} \tag{3.12}$$

$$\nu_t S^2 = \frac{C_{\omega 2}}{C_{\omega 1}} \frac{1}{f_\omega} \omega k \tag{3.13}$$

The turbulent viscosity, as expressed in Eq. (3.3), can be used to get an expression for the specific dissipation rate, ω.

$$\nu_t = C_\mu f_\mu \frac{k}{\omega} \qquad \Longrightarrow \qquad \omega = C_\mu f_\mu \frac{k}{\nu_t} \tag{3.14}$$

The subgrid scale turbulent kinetic energy can be expressed by combining Eq. (3.13) and (3.14).

$$k = \sqrt{\frac{C_{\omega 1}}{C_{\omega 2}} \frac{f_\omega}{C_\mu f_\mu}} \nu_t S \tag{3.15}$$

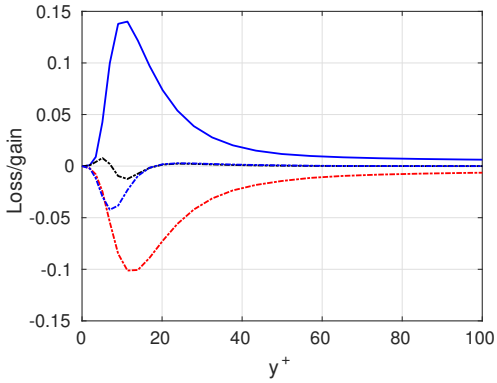

(a) k-eq., near-wall.

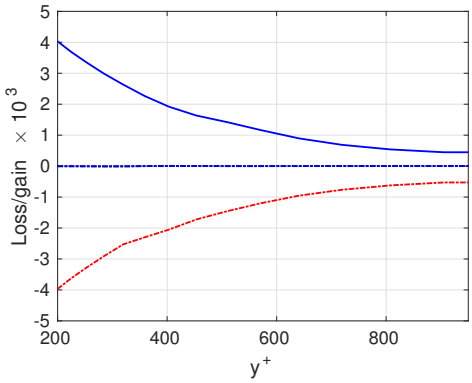

(b) k-eq., $y^+ \geq 200$.

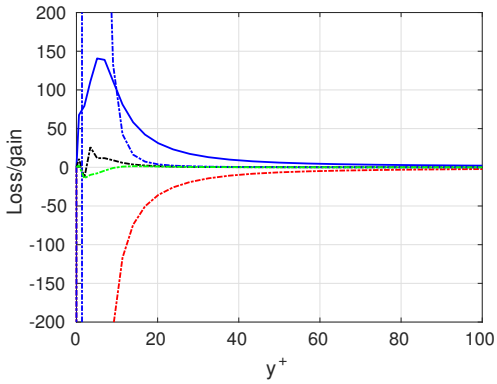

(c) ω-eq., near-wall.

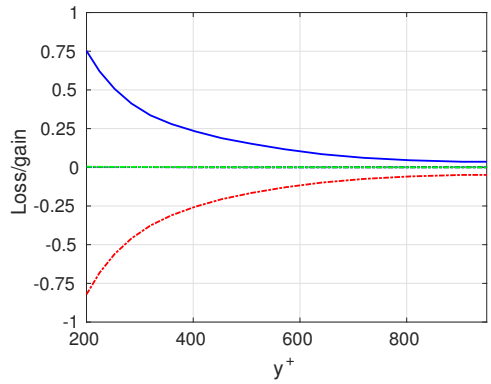

(d) ω-eq., $y^+ \geq 200$.

Figure 3.1: LES of fully developed channel flow, $Re_\tau = 950$. Budgets of subgrid-scale properties for PDH-LRN using Δ_{dw}. —— : production; - · - : dissipation/destruction; - - - : turbulent diffusion; - · - : viscous diffusion. - · - : cross diffusion. (a) and (b) k-equation, (c) and (d) ω-equation.

Inserting Eq. (3.15) in (3.12) forms an expression for the PDH-LRN Smagorinsky-like turbulent viscosity.

$$\nu_t = \frac{1}{f_k^2}\left(\frac{C_{\omega 2}}{C_{\omega 1}}\frac{C_\mu f_\mu}{f_\omega}\right)^{3/2}\left(\Psi_{PDH} C_{LES}\Delta\right)^2 S \tag{3.16}$$

Recapitulate Eq. (3.11) and identify the terms in Eq. (3.16). The expression for the function A_{PDH} can hence be written.

$$A_{PDH} = \frac{1}{f_k^2}\left(\frac{C_{\omega 2}}{C_{\omega 1}}\frac{C_\mu f_\mu}{f_\omega}\right)^{3/2} \tag{3.17}$$

As seen, A_{PDH} depends on the damping functions, which in turn are functions of the

local turbulent Reynolds number. To achieve $A_{PDH}\Psi_{PDH}^2 = const$, A_{PDH}^* is introduced to represent A_{PDH} when $R_t \to \infty$.

$$R_t \to \infty \Longrightarrow f_k,\ f_\omega,\ f_\mu \to 1$$

$$A_{PDH}^* = \left(\frac{C_{\omega 2}C_\mu}{C_{\omega 1}}\right)^{3/2} \tag{3.18}$$

In correspondence with A_{PDH}^*, we seek a function $\Psi_{PDH}^* = 1$, i.e. Ψ_{PDH} without any low Reynolds-number correction. The formulation of the correction function, including numerical limiters, can now be outlined.

$$\left(\frac{\Psi}{\Psi^*}\right)^2 = \frac{A^*}{A} \quad \Longrightarrow \quad \Psi_{PDH} = \min\left[10, f_k\left(\frac{f_\omega}{f_\mu}\right)^{3/4}\right] \tag{3.19}$$

The upper limit of Ψ is chosen according to Spalart et al. [11]. The damping functions and the derived correction function are plotted in Fig. 3.2 as a function of the turbulent Reynolds number.

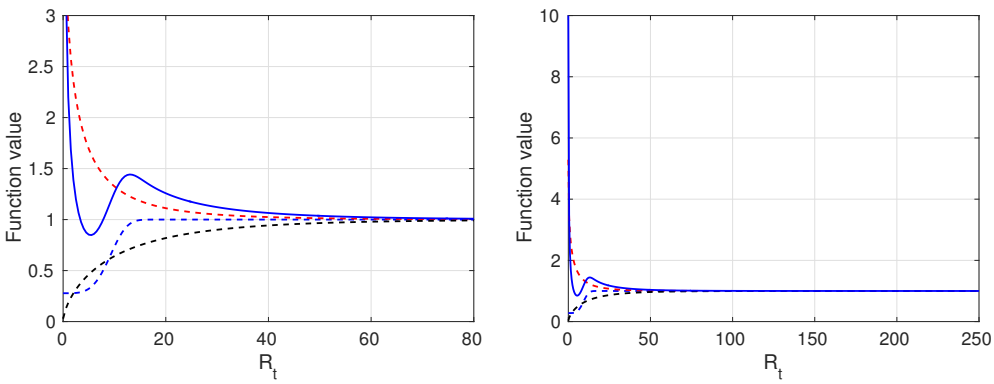

(a) Low R_t. (b) High R_t.

Figure 3.2: Damping functions and correction function used in PDH-LRN. - · - : f_k; - · - : f_ω; - · - : f_μ; —— : Ψ_{PDH}.

It is important to note that the flow is not in local equilibrium for $y^+ < 20$, see FIg. 3.1. Hence, due to the assumption made in the derivation of Ψ_{PDH}, the LES mode of the proposed hybrid RANS-LES method should not be applied very close to the wall. The proposed model should only be used as a hybrid RANS-LES, where RANS is applied for $y^+ < y^+_{limit}$, where $y^+_{limit} > 20$.

3.1.3 The LES length scale

Four different LES length scales from the literature have been evaluated in this thesis and are presented in Eqs. (3.20) to (3.23). There are two reasons for the evaluation. The first

is to find a LES length scale that in a zonal hybrid RANS-LES formulation can contribute to a reduction of the log-layer mismatch. The second is to find a suitable LES length scale that reduces the transition region from RANS to LES in free shear layer flows.

The motivation for various length scale formulations stems from different needs and is dependent on the flow condition considered. As mentioned above, the subgrid scale turbulent viscosity is proportional to the square of the LES length scale. Using different length scale formulations can thus significantly affect the level of turbulence viscosity produced by the model and, hence, the model's capability to resolve turbulence. A rapid formation of turbulence-resolving flow, when switching the hybrid RANS-LES model from RANS to LES, is a key issue in reducing the log-layer mismatch and mitigating the grey area. The LES length scale is therefore an essential component in hybrid RANS-LES modeling and important to address.

As motivated by Spalart et al. in the formulation of DES [6], Δ_{max} (Eq. 3.20) is chosen so that the boundary layer is protected from LES content and to reduce the risk for Modeled-Stress Depletion (MSD) and Grid-Induced Separation (GIS). Moreover, Spalart et al.[6] motivated the use of the local maximum cell size with the fact that the grid cannot resolve smaller turbulent scales than the local maximum grid size. Another commonly used length scale, especially in pure LES models, is based on the cubic root of the control volume (Eq. 3.21).

$$\Delta_{max} = \max\left(\Delta_x, \Delta_y, \Delta_z\right) \tag{3.20}$$

$$\Delta_{vol} = \left(\Delta_x \Delta_y \Delta_z\right)^{1/3} \tag{3.21}$$

Consequently, due to the relation between the subgrid scale turbulent viscosity and the filter width, the use of Δ_{max} on stretched grids will produce higher levels of turbulent viscosity compared to Δ_{vol}, which e.g. was highlighted by Breuer et al. [42]. The cell volume based LES length scale, Δ_{vol}, is also used in some modes of ZDES by Deck [9, 29] in order to speed up the formation of resolved turbulence. However, the use of Δ_{vol} was criticized by Spalart [54] due to its weak physical interpretation. Davidson and Peng also demonstrated the effect of a different filter width in their zonal formulation [7]. They motivated their choice of the minimum cell size, $\Delta = \min\left(\Delta_x, \Delta_y, \Delta_z\right)$, instead of Δ_{vol}, by a considerably better performance in channel flow.

The vorticity based LES length scale by Chauvet et al. [30] given by Eq. (3.22) is suitable for free shear layer flows since the filter width is adapted so that it aligns with the plane perpendicular to the local vorticity spin axis. Compared to Δ_{max} and Δ_{vol}, Δ_ω is advantageous if stretched grids are used in the free shear layer due to its lower turbulent viscosity. However, if cube sized grid cells are used, which is recommended in regions with separated flow, all three length scales reduce to $\Delta = \Delta_\Omega = \Delta_{vol} = \Delta_{max}$.

$$\begin{aligned} \Delta_\Omega &= \sqrt{N_x^2 \Delta_y \Delta_z + N_y^2 \Delta_x \Delta_z + N_z^2 \Delta_x \Delta_y} \\ N &= \frac{\Omega}{\parallel \Omega \parallel}, \qquad \Omega = \nabla \times u \end{aligned} \tag{3.22}$$

As mentioned in the introduction of this thesis, Shur et al. [12] proposed IDDES with the aim of achieving a non-zonal WMLES functionality where no log-layer mismatch is present. The LES length scale Δ_{dw} presented in Eq. (3.23) is an essential part of the IDDES formulation since it contributes very much to the reduction of the log-layer mismatch. In Shur et al. [12], they evaluated Δ_{dw} in LES of fully developed channel flow with the Smagorinsky model at $Re_\tau = 400$ and with an algebraic WMLES method at $Re_\tau = 18000$. In both simulations, Δ_{dw} gave a much improved prediction of the time-averaged velocity profiles compared to the standard LES length scale Δ_{vol}. However, for other Reynolds numbers, Shur et al. [12] state that Δ_{dw} does not work satisfactorily with regards to the log-layer mismatch and argue that more empiricism is needed, which resulted in the IDDES formulation [12]. In this thesis, Δ_{dw} is used with the proposed zonal hybrid RANS-LES model based on PDH-LRN. The LES length scale reads

$$\Delta_{dw} = \min\left(\max\left[C_{dw}d_w, C_{dw}\Delta_{max}, \Delta_{nstep}\right], \Delta_{max}\right) \tag{3.23}$$

where d_w is the wall distance, $C_{dw} = 0.15$, Δ_{nstep} is the grid cell size in the wall-normal direction and Δ_{max} is according to Eq. (3.20).

The Δ_{dw} length scale consists of three components: the near wall component, $\Delta_{dw} = C_{dw}\Delta_{max}$; the component related to the flow away from the wall $\Delta_{dw} = \Delta_{max}$ and the component bridging the two components as described below. As seen, Δ_{dw} returns the LES length scale used in DES and DDES in regions away from the wall, which is motivated by the facts that the small turbulent eddies are assumed to be statistically isotropic and that the grid in these regions should be designed so that $\Delta_{max} = \Delta_x = \Delta_y = \Delta_z$. The component bridging the near-wall and off-wall components is $\Delta_{dw} = C_{dw}d_w$ or alternatively $\Delta_{dw} = \Delta_{nstep}$ if $\Delta_{nstep} > C_{dw}d_w$. The LES length scale grows linearly in this bridging region, and the grid is preferably designed so that $\Delta_{dw} = C_{dw}d_w$. $\Delta_{dw} = \Delta_{nstep}$ is seen by Shur et al. [12] as an undesirable but necessary fallback in order not to let Δ_{dw} return too large a LES length scale if the grid is highly stretched (with a stretching ratio larger than $1 + C_w$) in the wall-normal direction.

The LES length scales described in this section have been applied to the flow cases described in Chapter 4. The length scales presented in Eqs. (3.20) to (3.23) have been applied to fully developed channel flow to evaluate their ability to reduce the log-layer mismatch. The wall distance based length scale, Δ_{dw} has also been applied to channel flow simulated as embedded LES, to the flow over a wall-mounted hump and to the spatially developing boundary layer flow. In the transonic duct flow, Δ_{dw} was applied but with Δ_{nstep} omitted as in Gritskevich et al. [23]. The arguments for omitting Δ_{nstep} are that its contribution is weak for properly designed hybrid RANS-LES grids and that this grid measure is not easily defined in unstructured solvers. An alternative to Δ_{nstep} in unstructured solvers is $\Delta_{\min} = \min(\Delta_x, \Delta_y, \Delta_z)$ since $\Delta_{\min}$ and Δ_{nstep} should be similar inside the boundary layer, presuming that strong grid refinement is not applied in the tangential wall directions. In the mixing layer flow, the effect of Δ_{max} and Δ_Ω on the RANS-to-LES transition region is evaluated.

3.2 RANS-LES interface methodologies

This section describes the RANS-LES interface methodologies used in this thesis. The purpose of the methodologies presented is to promote the development of resolved turbulence on the LES side of the interface in order to shorten the RANS-to-LES transition region.

3.2.1 Commutation error at the RANS-LES interfaces

A commutation error occurs in hybrid RANS-LES simulations since the hybrid filter does not commute with the spatial derivative. Due to the non-commutivity, an additional term appears when computing the spatial derivative of a physical quantity f, as shown in Eq. (3.24).

$$\frac{\overline{\partial f}}{\partial x_i} = \frac{\partial \overline{f}}{\partial x_i} - \frac{\partial \Delta}{\partial x_i}\frac{\partial \overline{f}}{\partial \Delta} \tag{3.24}$$

It has been shown that the commutation error can be large at the RANS-LES interface [38, 55]. In this thesis the effect of commutation terms at wall-normal and wall-parallel RANS-LES interfaces is explored in simulations of channel flow, hump flow, boundary layer flow and mixing layer flow. The two different RANS-LES interfaces are schematically shown in Fig. 1.4 in Section 1.3.

The commutation terms for the convection terms in the k and ω equations, based on Hamba's [38] derivation are used. Moreover, a commutation term for the convection term in the momentum equations is applied. Only the commutation error due to the switch of modeling mode at the RANS-LES interface is taken into account in this thesis. Due to the moderate stretching in the LES region of the grids used, the commutation error due to the non-homogeneous grid in the LES region is therefore neglected since this effect is assumed to be much smaller than the effect of switching the modeling mode.

Using Eq. (3.24), the commutation term, S_k^c, for the convection in the modeled k equation can be formulated as

$$\frac{\overline{\partial u_i k}}{\partial x_i} = \frac{\partial \overline{u}_i k}{\partial x_i} - \underbrace{\frac{\partial \Delta}{\partial x_i}\frac{\partial \overline{u}_i k}{\partial \Delta}}_{S_k^c} \tag{3.25}$$

A corresponding term can be formulated for the convection in the ω equation. The ω equation is derived by transforming the k and ϵ equations. It is assumed that the dissipation rate (ϵ) is not affected across the RANS-LES interface. This means that the viscous dissipation rate dominates over the viscous dissipation rate due to the resolved turbulence. Since the simulations presented are performed on grids much coarser than DNS resolution grids, which are required in order to achieve an accurate dissipation rate due to the resolved turbulence, the assumption is valid. To achieve the ω equation, start from the ϵ equation and multiply by $1/\left(C_k k\right)$

$$\frac{d\omega}{dt} = \frac{d}{dt}\left(\frac{\epsilon}{C_k k}\right) = \frac{1}{C_k k}\frac{d\epsilon}{dt} + \frac{\epsilon}{C_k}\frac{d(1/k)}{dt} = \frac{1}{C_k k}\frac{d\epsilon}{dt} - \frac{\omega}{k}\frac{dk}{dt} \tag{3.26}$$

From Eq. (3.26) it can be seen that the source term in the ω equation is given by the source term in the ϵ equation multiplied by $1/\left(C_k k\right)$ and the source term in the k equation multiplied by $-\omega/k$. This leads to the following commutation term in the ω equation

$$\overline{\frac{\partial u_i \omega}{\partial x_i}} = \frac{\partial \overline{u}_i \omega}{\partial x_i} - \frac{\partial \Delta}{\partial x_i}\frac{\partial \overline{u}_i \omega}{\partial \Delta} = \frac{\partial \overline{u}_i \omega}{\partial x_i} + \frac{\omega}{k}\frac{\partial \Delta}{\partial x_i}\frac{\partial \overline{u}_i k}{\partial \Delta} = \frac{\partial \overline{u}_i \omega}{\partial x_i} + \underbrace{\frac{\omega}{k} S_k^c}_{S_\omega^c} \tag{3.27}$$

By adding the commutation terms in the k and ω equations on the LES side of the RANS-LES interface, the aim is to reduce the RANS-to-LES transition region by reducing the turbulent viscosity on the LES side of the RANS-LES interface. The source term S_k^c, added to the k equation, acts to reduce the modeled turbulent kinetic energy for a flow across a RANS-to-LES interface. Since the source term in the ω equation has the opposite sign to the source term in the k equation, the commutation term increases the specific dissipation rate. Hence, for a flow across the interface with the direction from RANS to LES, a reduction of the turbulent viscosity will be obtained with a possibility to mitigate the grey area. With a flow from LES to RANS, the turbulent viscosity will be increased since the commutation terms will contribute to an increase in k and a reduction in ω.

The commutation term introduced in the k equation contributes to a change in the modeled turbulent kinetic energy across the RANS-LES interface. This change should be compensated with a change of the resolved turbulent kinetic energy. For example, when the modeled turbulent kinetic energy is reduced across a RANS-to-LES interface due to S_k^c, the resolved turbulent kinetic energy should be reduced by the same amount across the interface. This energy transfer is achieved by introducing a source term in the momentum equations, which should represent a commutation term in the transport equation for the resolved turbulent kinetic energy.

The transport equation for resolved turbulent kinetic energy is derived by subtracting the time-averaged momentum equations from the instantaneous momentum equations to get the momentum equations for a fluctuating velocity. Each term in this equation are multiplied by $\overline{u}_i'$ and time-averaged. The source terms introduced in the momentum equations are in this thesis based on the source term S_k^c, representing the commutation error for the convection term in the k_{sgs} equation. The time-average of the source term in the momentum equations for the fluctuating velocity multiplied by the velocity fluctuation should thus be found in the transport equation for resolved turbulent kinetic energy, i.e. $\langle S_k^c \rangle$. The source term introduced in the momentum equations can take the form

$$S_i^1 = S_k^c \frac{\overline{u}_i'}{\langle \overline{u}_m' \overline{u}_m' \rangle} \tag{3.28}$$

Consider now to multiply Eq. (3.28) with $\overline{u}_i'$ and time average

$$\left\langle S_k^c \frac{\overline{u}_i'}{\langle \overline{u}_m' \overline{u}_m' \rangle} \overline{u}_i' \right\rangle \simeq \langle S_k^c \rangle \frac{\langle \overline{u}_i' \overline{u}_i' \rangle}{\langle \overline{u}_m' \overline{u}_m' \rangle} = \langle S_k^c \rangle \tag{3.29}$$

where the correlation between S_k^c and $\overline{u}_i'$ is assumed to be weak. As seen, Eq. (3.29) is equal to the time-average of Eq. (3.25), but with opposite sign, as it should. The two terms have opposite signs, indicating that the enhanced turbulent fluctuations corresponds to a reduced modeled k_{sgs}.

To ensure that S_i^1 has the same sign as the velocity fluctuation itself in order to act as a modeled generator of turbulence at the RANS-LES interface and thus enforce the velocity fluctuations, the `sign` function is introduced. Finally, the used source term in the momentum equations reads

$$S^c_{mom,i} = \texttt{sign}\,(u_i') \left| S_k^c \frac{u_i'}{\langle u_m' u_m' \rangle} \right|. \tag{3.30}$$

A similar term was proposed by Davidson [40] and used in zonal PANS simulations of channel flow.

It should be noted that the introduction of $S^c_{mom,i}$ requires a running time-average in order to compute the velocity fluctuations. In the simulations presented in this thesis, typically 1000 time-steps were used to establish the time-averaged velocities from a fully developed flow. The number of time-steps needed to establish the flow with the source term introduced in the momentum equations differed between the simulated flows. Due to the periodicity in fully developed channel flow simulations, 10 000 time steps were needed to establish the interface fluctuations given by $S^c_{mom,i}$. In the embedded LES simulations of channel flow, boundary layer flow and mixing layer flow much fewer time-steps could be used since the turbulence is not recycled as in the simulations of fully developed channel flow. Typically, 1000 time steps were needed in the latter flow simulations.

The source term introduced in the momentum equations (Eq. (3.30)) is added only on the LES side of the interface, following the strategy to enforce the velocity fluctuations at the same time as the modeled turbulent kinetic energy (and the turbulent viscosity) is reduced by the source term introduced in the k (and ω) equation on the LES side of the interface.

It is important to note that the proposed methodology does not involve any empirical constants or functions. Moreover, it is a general method that can be applied to any transport equation based hybrid RANS-LES turbulence model. To discretize the source term S_k^c around the RANS-LES interface, a finite difference approximation is applied as in Hamba [38], see the sections below.

Wall-normal interface

In simulations where a wall-normal interface is used, as schematically shown in Fig. 1.4, the discretized form of S_k^c reads

$$\begin{aligned} S_k^c &= \frac{\partial \Delta}{\partial x}\frac{\partial \overline{u} k}{\partial \Delta} = \left(\frac{\Delta_{LES} - \Delta_{RANS}}{\Delta x}\right) \frac{\overline{u}_{RANS} k - \overline{u}_{LES} k_{LES}}{\Delta_{RANS} - \Delta_{LES}} \\ &= \frac{\overline{u}_{LES} k_{LES} - \overline{u}_{RANS} k}{\Delta x} \end{aligned} \tag{3.31}$$

where Δx is the distance between the cell centers at the RANS and LES locations, here indicated by the subscript $RANS$ and LES, respectively, on each side of the interface, as shown in Fig. 3.3.

The value of k_{LES} is the estimated SGS turbulent kinetic energy computed according to Eq. (3.32). The value of k (without any subscript in Eq. (3.31)) is set to the value at

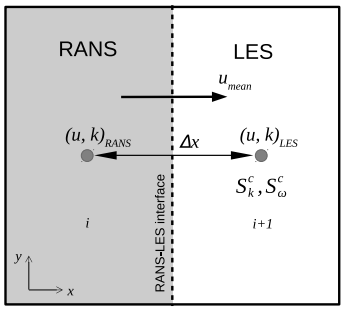

(a) Strategy 1.

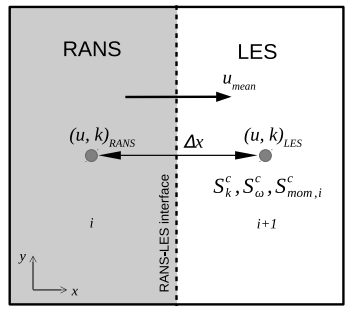

(b) Strategy 2.

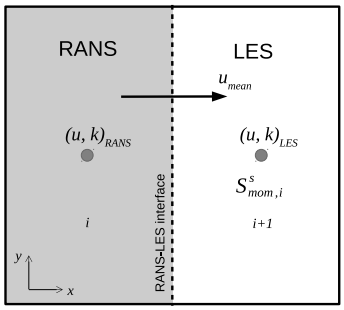

(c) Strategy 3.

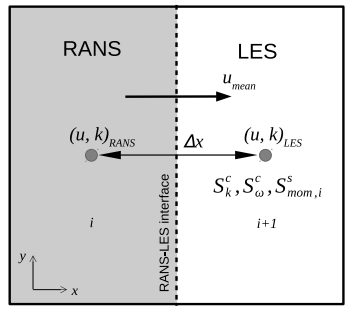

(d) Strategy 4.

Figure 3.3: Strategies for the wall-normal RANS-LES interface. RANS and LES cells, adjacent to the RANS-LES interface, with source terms for commutation error (S_k^c, S_ω^c and $S_{mom.i}^c$) and synthetic turbulent fluctuations ($S_{mom,i}^s$).

the current cell i, and not to its RANS value. This is done in order to achieve a smooth reduction of k across a RANS-to-LES interface and to avoid stability problems.

$$k_{LES} = \left(\frac{\nu_{sgs}}{\Delta}\right), \nu_{sgs} = (C_s\Delta)^2 \left|\overline{s}\right|, C_s = 0.1 \tag{3.32}$$

The filter width, Δ, used to estimate k_{LES} in Eq. (3.32) corresponds to the filter width used for the LES length scale in the dissipation term in the transport equation for the turbulent kinetic energy (Eq. (3.1)). It should be noted that there is no explicit dependency of Δ in Eq. (3.31)) since it is assumed that Δ and k varies linearly between the RANS and the LES locations. Hence, the RANS and LES length scales in the nominator and the denominator cancel each other. However, Δ is implicitly involved in S_k^c since it is assumed that k varies between Δ_{RANS} and Δ_{LES}.

Four combinations are presented in Fig. 3.3 for how the source terms representing the commutation error and synthetic turbulent fluctuations have been applied at the wall-normal RANS-LES interface in this thesis. In strategy 1, commutation terms are added in the k and ω equations in order to rapidly reduce the turbulent viscosity on the LES side of the RANS-LES interface. In strategy 2, commutation terms are added in

the k, ω and momentum equations. The source term in the momentum equations acts as a modeled turbulence generator in order to further promote the growth of the resolved turbulence. With strategy 3, synthetic turbulent fluctuations are added as source terms in the momentum equations ($S^s_{i,mom}$) at the wall-normal RANS-LES interface (or inlet plane) without any commutation terms. Strategy 4 uses the commutation terms in the k and ω equations to reduce the turbulent viscosity on the LES side of the interface, and synthetic turbulent fluctuations (see Section 3.2.2) are added to the momentum equations as source terms in order to speed up the formation of the turbulence resolving flow.

Table 3.1 shows applications in this thesis to which the different interface strategies have been applied. If no commutation terms are added in the k and ω equations and no synthetic turbulent fluctuations are added at the wall normal RANS-LES interface or the inlet plane, this is indicated by 0 in the table. The strategies used for the wall-parallel RANS-LES interfaces are also included. These strategies are described in the following section.

Table 3.1: Methodologies applied to the RANS-LES interfaces for different flow cases.

Flow case	Strategy for wall-normal interface or inlet plane	Strategy for wall-parallel interfaces
DHIT	N/A	N/A
Channel flow[1], Re_τ=8000	N/A	0, 1, 2, 3
Channel flow[2], Re_τ=950	4	N/A
Channel flow[2], Re_τ=8000	3, 4	0, 1, 2, 3
Hump	4	0
Boundary Layer	3, 4	0, 1, 2, 3
Mixing layer	0, 1, 2	N/A
Transonic duct flow	0	0

[1]Fully developed channel flow
[2]Channel flow simulated as embedded LES.

The influence of the distance Δx on the commutation terms in the k and ω equations has been analyzed by Davidson [56], where he concludes that the larger the Δx, the weaker the effect of the commutation terms. In this work, Δx is the distance between the adjacent cell centers at each side of the RANS-LES interface. Even though the proposed commutation term gives a strong impact on the production of the modeled turbulent kinetic energy with such a small distance Δ_x between the RANS and LES locations, this distance, between the adjacent cells, and this is also so for complex grids.

At a wall-normal RANS-LES interface, where the upstream flow is simulated with RANS and the downstream flow is simulated using a near-wall RANS layer and an off-wall LES region, as shown in Fig. 1.4, the commutation terms should, formally, only be added in the off-wall LES region since this is where the commutation error appears.

In hybrid RANS-LES simulations of e.g. channel flow with a near-wall RANS region, the turbulent viscosity in this region is less than the turbulent viscosity is when the flow is simulated only with RANS. This is because of the entrainment of LES content from then neighboring LES region in the former case, see e.g. Davidson [40]. From a modeling

point of view it could thus be argued that not only the turbulent viscosity in the LES region should be reduced across the wall-normal interface in embedded LES but also the turbulent viscosity in the near-wall RANS region. This reduction can be made using Eq. (3.31).

In this thesis, the commutation terms in the k and ω equations have been applied in both the near-wall RANS region and the off-wall LES region at embedded wall-normal interfaces and inlet boundaries. The argument is as described above: to reduce the turbulent viscosity also in the near-wall RANS region in order to rapidly adapt to the lower RANS turbulent viscosity given in the hybrid RANS-LES region. In these simulations, synthetic turbulent fluctuations are added at the RANS-LES interface in the near-wall RANS region.

Wall-parallel interface

A wall-parallel interface is shown schematically in Fig. 1.4. Similar to the discretization of the wall-normal interface, the wall-parallel interface is discretized as follows

$$\begin{aligned} S_k^c &= \frac{\partial \Delta}{\partial y}\frac{\partial \overline{v}k}{\partial \Delta} = \left(\frac{\Delta_{LES}-\Delta_{RANS}}{\Delta y}\right)\frac{\overline{v}_{RANS}k - \overline{v}_{LES}k_{LES}}{\Delta_{RANS}-\Delta_{LES}} \\ &= \frac{\overline{v}_{LES}k_{LES} - \overline{v}_{RANS}k}{\Delta y} \end{aligned} \tag{3.33}$$

As in Eq. (3.31), k_{LES} is computed according to Eq. (3.32) and k without any subscript is taken at cell j. Moreover, Δy is the distance between the cell centers adjacent to the RANS-LES interface. Note that it is assumed in Eq. (3.33) that the velocity v is positive across a RANS-to-LES interface. Thus, at the upper wall in the channel flow, the sign of S_k^c has to be taken care of so that this term acts as a sink term in the k equation for a flow going from RANS to LES.

In this thesis, three strategies for applying the commutation terms in the k, ω and the momentum equations at the wall-parallel RANS-LES interface have been evaluated, as shown in Fig. 3.4, where v_{int} is the velocity at the RANS-LES interface.

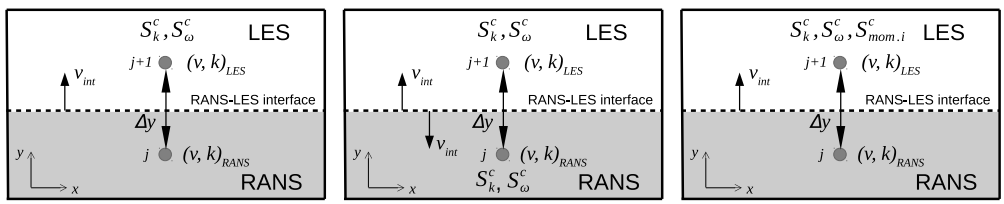

(a) Strategy 1. (b) Strategy 2. (c) Strategy 3.

Figure 3.4: Strategies for the wall-parallel RANS-LES interface. RANS and LES cells, adjacent to the RANS-LES interface, with source terms for commutation errors (S_k^c, S_ω^c and $S_{mom.i}^c$).

In the first strategy shown in Fig. 3.4 (a), the commutation terms in the k and ω equations have been applied only on the LES side of the interface when the flow direction across the interface is from RANS to LES. When the flow direction is from the LES to the RANS region, the commutation terms are set to zero. In the second strategy, as shown in Fig. 3.4 (b), the commutation terms have been added on both sides of the interface. When the direction of the flow across the interface is from the RANS to the LES region, the commutation terms on the LES side of the interface reduce the turbulent viscosity in the LES region. When the flow direction across the interface is from LES to RANS, the commutation terms are added on the RANS side on the interface in order to increase the turbulent viscosity in the RANS region. The third strategy shown in Fig. 3.4 (c) is similar to strategy 1, but the source term $S^c_{mom,i}$ in the momentum equations is added on the LES side of the interface. Table 3.1 in the previous section summarizes to which flow cases the different interface strategies have been applied. A 0 in Table 3.1, indicates that no commutation terms are added at the wall-parallel RANS-LES interfaces.

It was observed that, instantaneously, the magnitude of the commutation term in the momentum equations, $S^c_{mom.i}$, can take values of the same order as the magnitude of the convection term and the diffusion term, which caused stability problems. Therefore, in the simulation where $S^c_{mom.i}$ is applied at the wall-parallel interface, the commutation term in the momentum equations has been limited to the minimum of the magnitude of the convection and diffusion terms.

Due to the formulation of the RANS flux ($v_{RANS}k$) for the turbulent kinetic energy in Eq. (3.33) and the fact that the modeled turbulent kinetic energy is larger on the RANS side of the interface than on the LES side, the contribution from the commutation terms will be stronger on the RANS side of the interface than on the LES side.

3.2.2 Synthetic turbulence

Synthetic turbulent fluctuations (STF) are superimposed onto the RANS mean flow field at the interface in order to trigger the equations to resolve turbulence and to reduce the RANS-to-LES transition region. In this thesis, STF are imposed on embedded wall-normal RANS-LES interfaces as well as on inflow boundaries. The flow cases to which STF have been applied in this thesis are presented in Table 3.1 above.

Anisotropic synthetic turbulent fluctuations, based on a modified von Karman spectrum, are used in this thesis. The methodology used to generate the STF is presented in the work by Davidson [40, 57] and Davidson and Peng [32].

Two different approaches have been used to apply the STF in the simulations. When the STF are applied at an inlet boundary, as in the boundary layer simulations and the simulations of the hump flow, the STF are added directly to the mean velocities in the inlet boundary condition. In simulations in which STF are applied to an embedded wall-normal interface, as in the simulations of channel flow, the STF are applied as source terms in the momentum equations. With the addition of STF, turbulent kinetic energy is added to the simulation. To avoid an excess of turbulent kinetic energy at the LES side of the interface, the modeled turbulent kinetic energy on the LES side of RANS-LES interface has been manipulated either by a prescribed constant, $f_{k,int}$, as in paper B, or with the use of commutation terms, as in paper D-F, as shown in Fig. 3.3 (d).

The procedure for generating the STF is summarized below.

1. A precursor RANS simulation is made using the PDH-LRN model [48] in order to get profiles of velocities, turbulent kinetic energy and specific dissipation rate at the inlet or at the embedded wall-normal interface to which the STF should be applied.

2. Choose a suitable Reynolds stress tensor.

3. The Reynolds stress tensors and the turbulent length scale $l_{t,s}$ are used as input for the generation of the synthetic turbulence.

4. The synthetic turbulence generator assumes homogeneous turbulence, hence the Reynolds stress tensor can be prescribed only in one point. In this thesis STF are applied only to attached boundary layers where the shear stress is the most important stress component. Therefore, the Reynolds stress tensor is chosen at the point where the turbulent shear stress is largest.

5. As a last step, the turbulent fluctuations are scaled based on the profiles from the precursor RANS simulation.

The Reynolds stress tensor in step 2 in the list above is taken in paper B from DNS of fully developed channel flow. In papers D-F, the Reynolds stress tensor is computed from the Wallin and Johansson EARSM model [58] using u, k and ω from the precursor RANS simulation.

At step 3 above, the turbulent length scale $l_{t,s} = 0.5\delta_{in}$ and $l_{t,s} = 0.8\delta_{in}$ were used for the embedded LES of channel flow and hump, respectively, in paper B, where δ_{in} is the boundary layer thickness at the embedded RANS-LES interface/inlet location and is taken from a precursor RANS simulation. In paper D, $l_{t,s} = k^{(3/2)}/\omega$, where k and ω are taken from the precursor PDH-LRN RANS simulation. This turbulent length scale gave good results in the simulations of channel flow and hump flow. However, it was observed in papers E and F that $l_{t,s} = k^{(3/2)}/\omega$ gave too small a turbulent length scale for the simulated boundary layer flow. Therefore, $l_{t,s} = 0.22\delta_{in}$, was chosen for all simulations in these two papers.

As the last step in the procedure for generating the STF, scaling of the fluctuations is used in order to mimic the actual flow characteristics as well as possible. No scaling was applied for the channel flow in paper B. For the hump flow in paper B, the STF was scaled using the PDH-LRN profile for the turbulent kinetic energy, $(k/k_{max})_{RANS}$. In paper D-F, the STF were scaled using the maximum shear stress, $\left(\left|\overline{u'v'}\right| / \left|\overline{u'v'}\right|_{\max}\right)^{1/2}_{RANS}$, which was taken from the precursor RANS simulation.

To compute the time correlation for the synthetic turbulence generator used described in [57], the bulk velocity and the turbulent length scale $l_{t,s}$ are used. Thus, no additional parameters are needed than those described in the list above. It should be noted that, with the commutation terms combined with the procedure described for generating STF, the only "free" parameter in the RANS-LES interface method used is the turbulent length scale.

4 Flow cases for calibration and validation

This chapter summarizes the flow cases used in the thesis for calibration and validation of the proposed zonal hybrid RANS-LES approach. A brief introduction describing the purpose and motivation is given for each flow case, and the most important outcomes are presented.

The simulations of the transonic flow in a rectangular duct have been performed with the unstructured compressible flow solver Edge, see Section 2.2. All other flow cases have been simulated using the incompressible structured flow solver CALC-LES presented in Section 2.1.

4.1 Transonic flow in a rectangular duct

Shock/boundary-layer interaction (SBLI) flows are commonly encountered in aeronautical applications and appears e.g. in phenomena such as buffeting on aircraft wings and in high-speed inlet configurations. For high-speed inlets, SBLI can typically take place inside the inlet duct, which can have a severe impact on the engine/inlet stability if it is not controlled.

Transonic flow in ducts is often associated with SBLI and flow separation in the duct corners. It has been found to be challenging to use CFD methods to predict such flows, especially using hybrid RANS-LES and DES methods, which was shown in e.g. papers A and C.

The present flow case is formed by a rectangular duct with a convergent-divergent nozzle used to accelerate the flow from subsonic speed to supersonic speed. A λ-shape shock wave downstream of the nozzle at Mach 1.4 interacts with the boundary layer, which consequently leads to local recirculation bubbles in the duct corners, as shown in Fig. 4.1. The walls are parallel in the shock region and the cross-sectional area is constant with $H = 178$ mm and $W = 117$ mm in height and width, respectively. The center line length of the duct is $L = 1030$ mm.

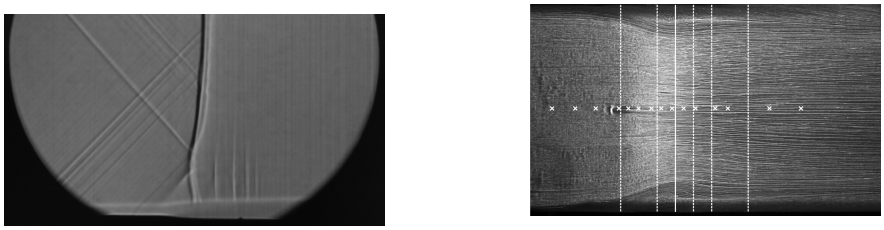

(a) Side view of shock wave with λ-foot.

(b) Oil-flow visualization on bottom wall.

Figure 4.1: Experiment. Flow from left to right. Visualization of (a) shock wave and (b) shock-induced corner separation bubbles. In (b), the third line from left indicates the shock location. Crosses indicate locations where wall pressures were measured.

The computational domain can be seen in Fig. 4.2. Two computational grids have been

used, one coarse and one fine. The fine grid is shown in Fig. 4.2, where the RANS and LES zones used in the simulations with the proposed zonal hybrid RANS-LES model are also indicated. The grids are of a hexahedral type with about 3.2 and 7.6 million nodes, respectively, in the different grids. Both grids have a refined region in the streamwise ($x-$) direction to resolve the shock wave. For both grids, the first wall-normal grid node is generally located at $y^+ < 2$. Compared to the coarse grid, the number of nodes in the wall-normal directions in the fine grid is doubled in the bulk region.

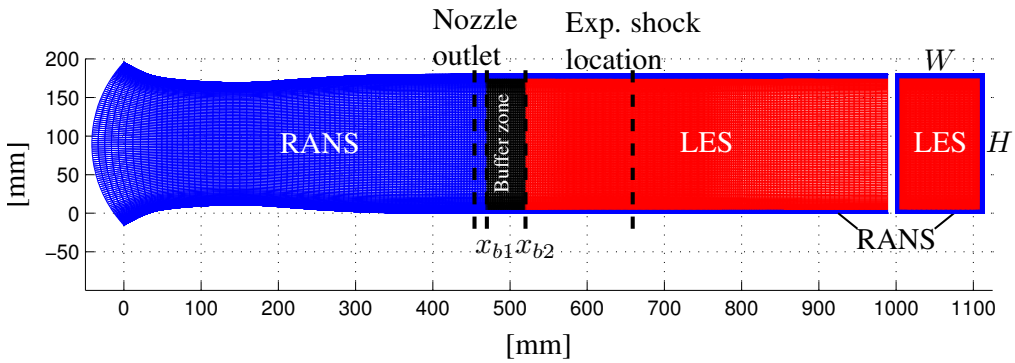

Figure 4.2: Computational grid with RANS and LES zones used in PDH-LRN based zonal RANS-LES simulations. Blue: RANS; black: buffer zone; red: LES. Left grid: xy-plane, flow from left to right. Right grid: yz-plane, grid cross-section.

The zonal hybrid RANS-LES simulations performed with the proposed model are made as follows. A buffer zone, in which the turbulent length scale is gradually switched from RANS to LES, is defined in between the RANS and the hybrid RANS-LES zones. The buffer zone helps to eliminate possible discontinuities in the transition from RANS to LES mode and is patched between x_{b1} and x_{b2} in the streamwise direction upstream of the shock. In simulations $x_{b1} = 470$ mm and $x_{b2} = 520$ mm, see Figs. 4.2 and 4.4 (a). The LES length scale $\Delta = \Delta_{dw}$ was used in the LES region, as described in Section 3.1.3.

Bottom-wall pressures and streamwise velocities in the duct center plane are available from the experiment [59]. Velocity profiles and wall pressure distributions from the simulations are compared to the experiment in papers A and C at a distance of Δx relative to the shock location, as illustrated by the lines in Fig. 4.1 (b). Only a comparison of wall-pressure distributions is presented in this extended summary. Measured at the center line of the duct, the shock wave in the experiment occurs at $x = 659$ mm ($\Delta x = 0$), i.e. 205 mm downstream of the nozzle exit. The Reynolds number, based on the displacement thickness and the local freestream velocity, U_0, at $\Delta x = -30$ mm is $Re_{\delta^*} = 13\ 600$.

Current state-of-the-art hybrid RANS-LES models have been applied to the present SBLI flow case and are compared to the proposed hybrid RANS-LES method based on the PDH-LRN $k-\omega$ model [48]. The turbulence models applied are given in Table 4.1 together with the computational grids used.

In addition to the hybrid RANS-LES methods applied to the present SBLI flow case,

Table 4.1: Turbulence models and grids used in simulations of the SBLI duct flow.

Turb. model	Type	Grid
PDH-LRN $k-\omega$	HRLM, zonal	fine
SA-DES	HRLM, non-zonal	coarse
SA-DDES	HRLM, non-zonal	fine
SA-DDES	HRLM, non-zonal	coarse
SA-IDDES	HRLM, non-zonal	fine
HYB0, zero-eq.	HRLM, non-zonal	fine
HYB0, zero-eq.	HRLM, non-zonal	coarse
PDH-LRN	RANS	coarse
Hellsten's $k-\omega$ + EARSM	RANS	coarse
Spalart-Allmaras one-eq.	RANS	coarse
Menter's SST $k-\omega$	RANS	coarse

different RANS models were evaluated. It was concluded that well established RANS models, such as the Spalart-Allmaras one equation model [20] and Menter's SST $k-\omega$ model [21], failed to accurately predict the SBLI flow. Both models predict an unphysical asymmetric flow field and a collapsed shock wave, which have also been shown by Bruce et al. [60]. Both Hellsten's $k-\omega$ model [61] combined with EARSM [58] and the low-Reynolds-number $k-\omega$ model by Peng et al. [48] predicted the pressure distribution across the shock reasonably well in the center plane of the duct. However, among the RANS models evaluated, the local corner separation bubbles were best predicted using the PDH-LRN model. The PDH-LRN model was therefore chosen as the background RANS model in the proposed hybrid zonal RANS-LES model.

The λ-shaped shook wave and the wall pressure distribution across the shock given by the proposed hybrid zonal RANS-LES model are shown in Fig. 4.3. The shape of the instantaneous shock wave is in good agreement with experimental data given in Fig. 4.1 (a). As shown in the time-averaged wall pressure distribution across the shock (Fig. 4.3 (b)), weak secondary shocks are present with the proposed hybrid RANS-LES model. This is due to the slightly over-predicted corner separation bubbles shown in Fig. 4.4 (a), which contributes to an enhanced flow acceleration to supersonic flow and the weak secondary shocks downstream of the main shock. The secondary shocks are not observed in the wall pressure distribution from the experiment, but can be noticed in the Schlieren visualization in Fig. 4.1 (a). Using SA-IDDES on the other hand, a much more unsteady shock is predicted giving a less distinct pressures rise across the shock as seen in Fig. 4.3 (b). An unphysical collapsed shock is given with SA-DDES and HYB0 (not shown) leading to the prolonged and weak pressure rise across the shock.

Using IDDES, most of the corner separation bubbles are simulated in LES mode (not shown here, but shown in paper C). With the proposed model, the RANS and LES zones are prescribed so that only the outer part of the corner separation bubbles are simulated in LES, which seems to be advantageous for the grid used. Since the grid resolution is very fine in the duct corners, as can be seen in Fig. 4.2, IDDES switches to its WMLES mode but the proposed model is kept in (U)RANS mode. However, the grid is probably not

(a) Side view of shock wave with λ-foot.

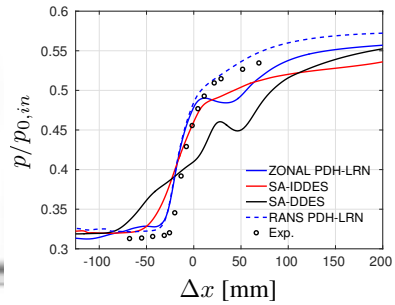

(b) Wall pressure.

Figure 4.3: Shock characteristics. (a) Instantaneous shock pattern at duct center plane using zonal PDH-LRN. Visualized as the magnitude of density gradients. (b) Time-averaged wall pressure along centerline across the shock using the fine grid.

fine enough to support the high level of resolved turbulence needed in the WMLES mode of IDDES to compensate for the low turbulent viscosity level (modeled turbulence) given by the model. Hence, the more pronounced shock motion observed in the SA-IDDES simulations is probably related to the poor modeling of the corner separation bubbles.

Even though the inner part of the corner separation bubbles is simulated in RANS mode with the proposed model, a large part of the highly turbulent flow downstream of the shock is resolved, as can be seen in Fig. 4.4 (b), where the Q-criterion has been used to visualize the resolved turbulent structures.

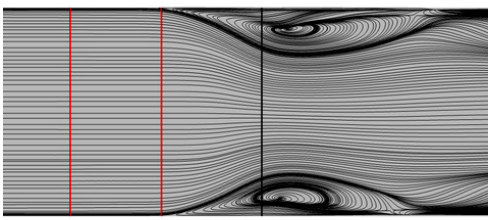

(a) Surface streamlines at bottom wall.

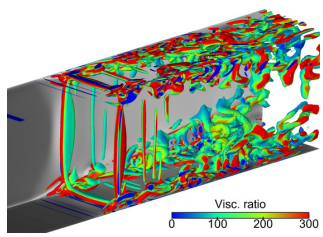

(b) Q-criterion, $QH^2/U_0^2 = 1$.

Figure 4.4: PDH-LRN based zonal RANS-LES using the fine grid. (a) Time-averaged surface streamlines in the SBLI region. Black line indicates shock location. Red lines indicate the buffer zone shown in Fig 4.2. (b) Resolved turbulent structures with skin friction displayed on the duct walls.

4.2 Decaying Homogeneous Isotropic Turbulence

The constant C_{LES} used in the LES mode of the proposed hybrid RANS-LES model was calibrated using Decaying Homogeneous Isotropic Turbulence (DHIT). Experimental data

by Comte-Bellot and Corrsin [62] were used as the reference.

DHIT was computed on two grids to investigate the effect of grid density on C_{LES}. Each grid, with a domain size of $(2\pi)^3$, consisted of 32^3 and 64^3 cubic shaped cells, respectively. Periodic boundary conditions were applied in all directions, and the simulation was initiated with a prescribed velocity field with zero mean velocity.

To reach adequate start values for k and ω, 4000 iterations were computed with a frozen velocity field, which was used as an initial condition for the unsteady DHIT simulation. The simulations were performed using a second order central differencing scheme for the continuity and momentum equations and a first order hybrid scheme for the k and ω transport equations. The initial velocity fields were generated by a widely used computer program from the group of Professor Strelets in St. Petersburg. Spectra are presented at two non-dimensional time steps: $T = 0.87$ and 2.0.

The criteria used to select the best suited C_{LES}-value are according to Bunge [63]. In short, this means that the 32^3 grid is given priority over the 64^3 grid. The 32^3 grid is seen as more representative for grids used in practical hybrid RANS-LES simulations of complex geometries/flows. Furthermore, $T = 2$ has precedence over $T = 0.87$.

Energy spectra from DHIT simulations at two different time-steps using the proposed model with $C_{LES} = 0.70$ are presented in Figure 4.5.

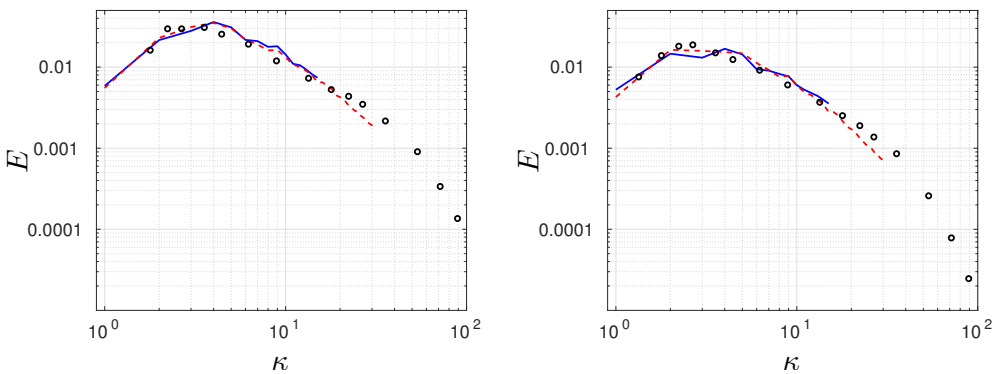

(a) $T = 0.87$ (b) $T = 2$

Figure 4.5: Energy spectra from DHIT using the LES mode of the PDH-LRN based hybrid RANS-LES model, $C_{LES} = 0.70$. —— : 32^3 grid; - - - : 64^3 grid; ∘: Experiments [62].

The simulations presented show, according to the selection criteria, that $C_{LES} = 0.70$ is the best value for the proposed model. Moreover, it is noted that the calibrated C_{LES}-value is very similar to other well known base RANS models used for hybrid RANS-LES modeling, such as the Spalart-Allmaras one equation model [20] and Menter's SST $k - \omega$ model [21].

4.3 Fully developed channel flow

Fully developed channel flow has been simulated at a Reynolds number based on friction velocity, $u_\tau = \sqrt{\tau_w/\rho}$, and half channel height δ equal to $Re_\tau = u_\tau \delta/\nu = 8000$. The purpose of this test case is to validate that the proposed model resolves turbulence in a wall-bounded flow. Moreover, an assessment of different LES length scales and commutation terms applied at the RANS-LES interface is made with the proposed model in order to evaluate the model's sensitivity to log-layer mismatch and how different RANS-LES interface methodologies can be used to remedy this issue.

The computational domain used in the simulations has dimensions of $(x, y, z)/\delta = (3.2, 2, 1.6)$ with a grid resolution of $(n_x, n_y, n_z) = (64, 96, 64)$ cells. In viscous units, the grid reads $(\Delta x^+, \Delta y^+, \Delta z^+) = (400, 1.7 - 1050, 200)$. Periodic boundary conditions are applied in the streamwise and spanwise directions, as seen in Fig. 4.6.

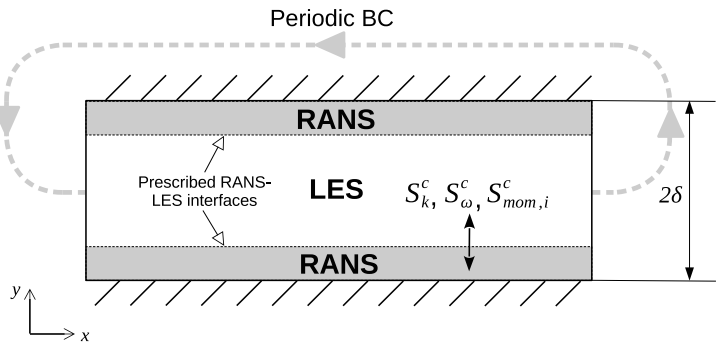

Figure 4.6: Computational setup for fully developed channel flow.

To verify the sensitivity of the domain size, two additional grids were used with the dimensions $(x, y, z) = (6.4, 2, 1.6)$ and $(3.2, 2, 3.2)$, where the same Δx^+, Δy^+ and Δz^+ values are used as for the above grid. Comparisons (not shown) of time-averaged streamwise velocity profiles, turbulent viscosity and modeled and resolved turbulent shear stress on the three grids show negligible differences. All results presented in this thesis are computed on the small domain.

The zonal formulation was chosen to evaluate the influence of the switch location on the log-layer mismatch. The RANS-LES interface was prescribed at four locations: $y^+ = 130$, $y^+ = 270$, $y^+ = 550$ and $y^+ = 1120$ (indicating the cell face) and the influence of the LES length scales Δ_{max}, Δ_{vol}, Δ_Ω and Δ_{dw} (Eqs. (3.20) to (3.23)) was evaluated. As highlighted in Section 3.2.1, the commutation error across the RANS-LES interface can be large. The effect of commutation terms in the k, ω and momentum equations, indicated by S_k^c, S_ω^c and $S_{mom.i}^c$ in Fig. 4.6, was therefore evaluated at the RANS-LES interfaces.

The effect of different LES length scale on the log-layer mismatch is shown in Fig. 4.7 (a). It can be concluded that Δ_{dw}, is superior to the other LES length scales evaluated in reducing the log-layer mismatch. A distinct log-layer mismatch is given by the three

other LES length scales. With Δ_{dw}, the most rapid reduction of the turbulent viscosity is given across the RANS-to-LES interface (not shown), which contributes to the quick development of the resolved turbulent shear stress shown in Fig. 4.7 (b). It can be observed that Δ_{vol} and Δ_{Ω} performs in a similar way, whereas Δ_{max} considerably degrades the model's capability to develop resolved turbulent shear stress on the LES side of the RANS-LES interface. The lower level of resolved shear stress given by Δ_{max} is also reflected in the velocity profile, where a more pronounced log-layer mismatch is given with this LES length scale.

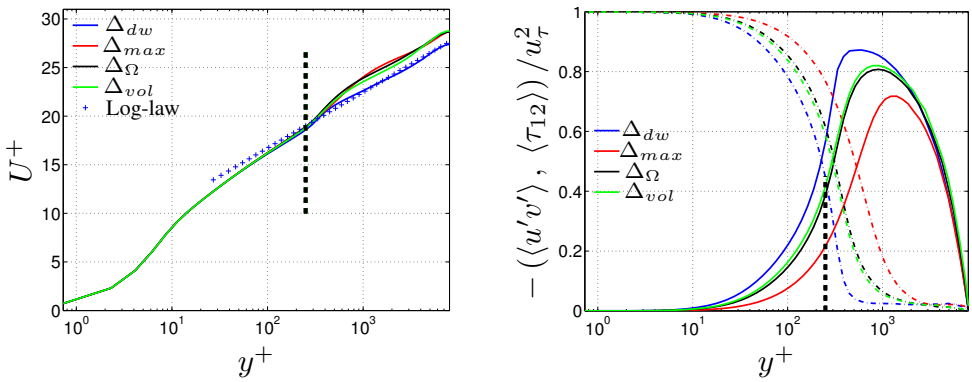

(a) Different LES length scales.

(b) Different Δ, $y^+_{switch} = 250$.

Figure 4.7: Fully developed channel flow, $Re_\tau = 8000$. Comparison of different LES length scales, $y^+_{switch} = 270$ (indicated by black dashed line). (a) Streamwise time-averaged velocity. (b) Resolved (solid) and molded+viscous (dash-dotted) turbulent shear stress.

For all the LES length scales evaluated, there is a tendency towards an increased log-layer mismatch when the RANS-LES interface is moved closer to the wall, as can be seen in paper B. With $\Delta = \Delta_{dw}$, the effect of the interface location on the log-layer mismatch is weak, as seen in Fig. 4.8 (a), which is an important aspect from a modeling robustness point of view. With the RANS-LES switch located at $y^+ = 270$, as shown in Fig. 4.7 (a), the centerline velocity is over-predicted, due to the log-layer mismatch, by about 6% for Δ_{max}, Δ_{vol} and Δ_{Ω} but only by 1% for Δ_{dw}. With the RANS-LES switch located at $y^+ = 130$ (not shown), the over-prediction of the centerline velocity is as high as 11% for Δ_{vol} and Δ_{Ω} but only 1.5% for Δ_{dw}. It can thus be concluded that among the LES length scales evaluated, the wall distance based LES length scale Δ_{dw} best reduces the log-layer mismatch and is the most robust with respect to the location of the wall-parallel RANS-LES interface. Therefore, Δ_{dw} is seen as the most suitable LES length scale for wall-bounded flows and is applied in such flows in this thesis.

Even though Δ_{dw} reduces the log-layer mismatch, a weak log-layer mismatch is still present. Therefore, the methodology based on commutation terms applied at the RANS-LES interface, following the recommendation by Hamba [38] described in Section 3.2.1, has been explored. The commutation terms presented in Eq. (3.25), (3.27) and (3.30) were applied. The effect of the commutation terms on the streamwise velocity profiles is

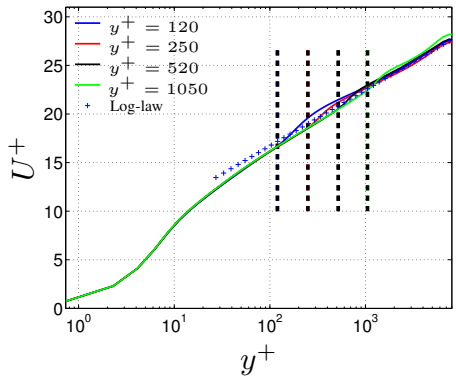

(a) Δ_{dw} at different y^+_{switch}.

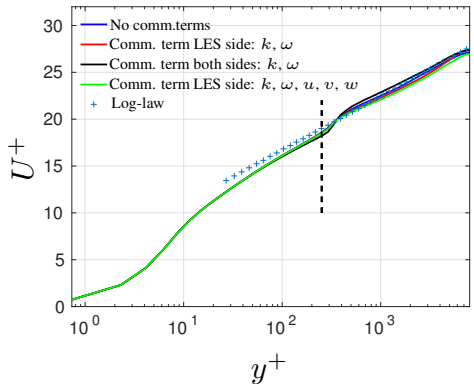

(b) Effect of commutation term.

Figure 4.8: Fully developed channel flow, $Re_\tau = 8000$, using $\Delta = \Delta_{dw}$. Streamwise time-averaged velocity. Switch locations indicated by black dashed lines. (a) Comparison between different RANS-LES switch locations. (b) Effect of commutation terms, $y^+_{switch} = 270$

presented in Fig. 4.8 (b). A slight improvement is seen when the commutation terms is applied on the LES side of the interface for both Δ_{dw} and the other LES length scales evaluated. Applying the commutation terms on both the RANS and LES sides of the interface gives a greater log-layer mismatch with Δ_{dw}. A similar trend is also observed for the other LES length scales evaluated as can be seen in paper E.

The effect of the commutation terms in the momentum equations is weak, and only marginal differences are seen between the simulations where the commutation terms are applied on the LES side of the interface in the k and ω equations and the k, ω and momentum equations, respectively. The weak effect of the commutation terms in the momentum equations is explained by the restriction needed on this term to avoid numerical instabilities as described in Section 3.2.1.

Finally, it can be concluded that the effect of the LES length scale dominates over the effect of the applied commutation terms with regard to log-layer mismatch, even though the commutation terms applied contribute to further alleviating the log-layer mismatch. Moreover, it has been shown that Δ_{dw} is superior to other LES length scales presented in literature when applied to channel flow.

4.4 Channel flow simulated as embedded LES

Channel flow at $Re_\tau = 950$ and 8000 was simulated using an embedded LES approach. An upstream RANS region is coupled with a downstream hybrid RANS-LES region, as shown in Fig. 4.9, or with a full LES region. Across the embedded RANS-LES interface, the RANS level of turbulent kinetic energy and specific dissipation rate is manipulated to match the downstream SGS levels. To speed up the establishment of the downstream turbulence-resolving LES flow, synthetic turbulent fluctuations are applied

at the embedded RANS-LES interface.

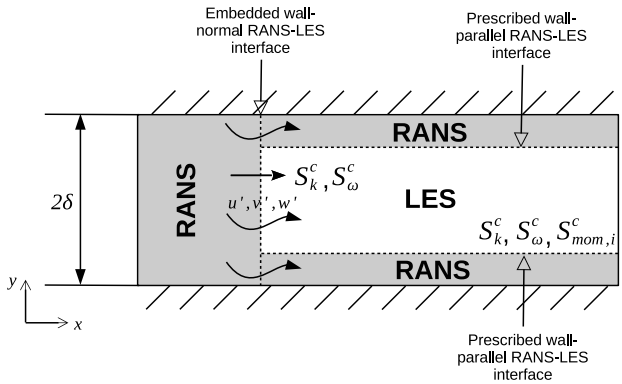

Figure 4.9: Channel flow simulated as embedded LES. Computational domain with interfaces.

The main purpose of this flow case is to evaluate the proposed model in a wall-bounded flow where synthetic turbulent fluctuations are added to the mean flow field at a wall-normal RANS-LES interface. The flow case has also been used to evaluate different RANS-LES interface methodologies for mitigating the grey area in embedded LES simulations.

The profiles of u, k and ω, taken from precursor PDH-LRN RANS simulations of fully developed channel flow were applied at the inlet boundary. Two different interface methodologies were used in the simulations for $Re_\tau = 950$. Firstly, in paper B, the amount of subgrid scale turbulent kinetic energy and specific dissipation rate was prescribed. The evaluated ratio of LES subgrid scale turbulent kinetic energy to RANS turbulent kinetic energy was in the range of $0.05 \leq f_{k,int} \leq 0.20$. Moreover, the added synthetic turbulent fluctuations in paper B had a constant distribution of the normal stresses across the embedded RANS-LES interface. The distribution of the shear stress was constant across the interface but with a changed sign for the upper half of the channel. Secondly, in papers D and F, commutation terms in the k and ω equations were applied at the wall-normal RANS-LES interface instead of the prescribed ratio of SGS to RANS turbulent kinetic energies. Furthermore, the synthetic turbulent fluctuations were scaled with the shear stress profile from the precursor RANS simulation of fully developed channel flow. In all simulations, $\Delta = \Delta_{dw}$ is used in LES mode.

In the simulations at $Re_\tau = 950$, the region downstream of the embedded RANS-LES interface was simulated without any near-wall RANS layer. This flow case was used to validate the simulation approach with DNS data as a reference. The simulations at $Re_\tau = 8000$ summarize both the wall-normal and wall-parallel RANS-LES interface methods used in this thesis. This Reynolds number is also more relevant for full scale industrial applications and are therefore presented in this extended summary.

Expressed in viscous units, the grid for $Re_\tau = 8000$ reads $(\Delta x^+, \Delta y^+, \Delta z^+) = (400, 0.7 - 980, 200)$. The wall-normal and spanwise dimensions are $\left(l_y, l_z\right)/\delta = (2, 1.6)$ with $\left(n_y, n_z\right) = (96, 64)$ cells. Streamwise domain lengths of $l_x/\delta = 12.8$ and 25.6 were

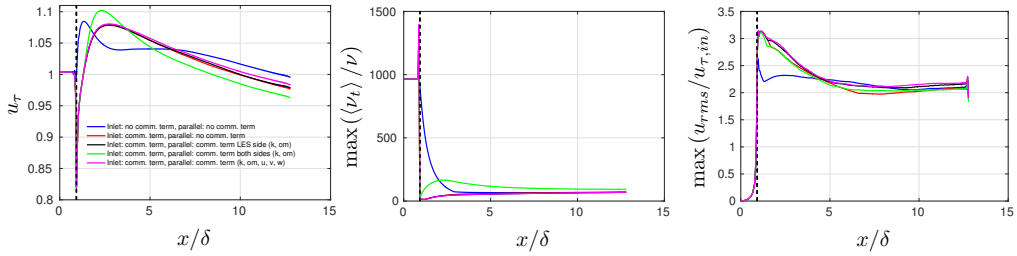

(a) Friction velocity. (b) Turbulent viscosity. (c) Normal stress.

Figure 4.10: Channel flow using embedded LES, $Re_\tau = 8000$. Effect of embedded wall-normal RANS-LES interface. Colors in (a) apply for all sub-figures. Dashed black line indicates the wall-normal interface.

computed with $n_x = 256$ and 512 cells, respectively, in order to reach a fully developed channel flow. Results for $n_x = 256$ is presented in this extended summary. Results for $n_x = 512$ is included in paper F.

The impact of the commutation terms and the synthetic turbulent fluctuations at the wall-normal interface is strong as shown in Fig. 4.10. A rapid reduction of the turbulent viscosity is obtained across the interface due to the commutation terms, and a rapid growth of the resolved turbulent stresses is given for the downstream flow due to the synthetic turbulence.

The commutation term is compared to the production term, P^k, in the k equation at the wall-normal and wall-parallel interfaces, in Fig. 4.11. The commutation term at the wall-normal interface is stronger than the commutation term added at the wall-parallel interfaces. Except at the peak of the production term in the k equation, the commutation term at the wall-normal interface is as large as 10-15 times the production term, which explains the strong reduction of the turbulent viscosity across the interface. Moreover, a much stronger reduced magnitude of the production term in the k equation is observed when the commutation terms in the k and ω equations are applied at the wall-normal interface than in the reference simulation, where no commutation terms are applied. The small peaks observed in the commutation term at the wall-normal interface at $y^+ = 550$ is a consequence of the commutation terms applied at the wall-parallel interface.

It can be concluded from the simulations presented that the commutation terms evaluated do not give a clear advantage with respect to grey area mitigation over the simulation in which no commutation terms are applied. None of the simulations reach a fully developed state. However, the slope of the friction velocity far downstream of the wall-normal interface is similar in all simulations, indicating that the recovery lengths also should be similar. Moreover, it has been shown that the commutation terms effectively reduce the turbulent viscosity on the LES side of the RANS-LES interface and that the added synthetic turbulent fluctuations rapidly establish a turbulence-resolving LES flow. This was also shown in Davidson [41], where commutation terms were applied in the k and ω equations.

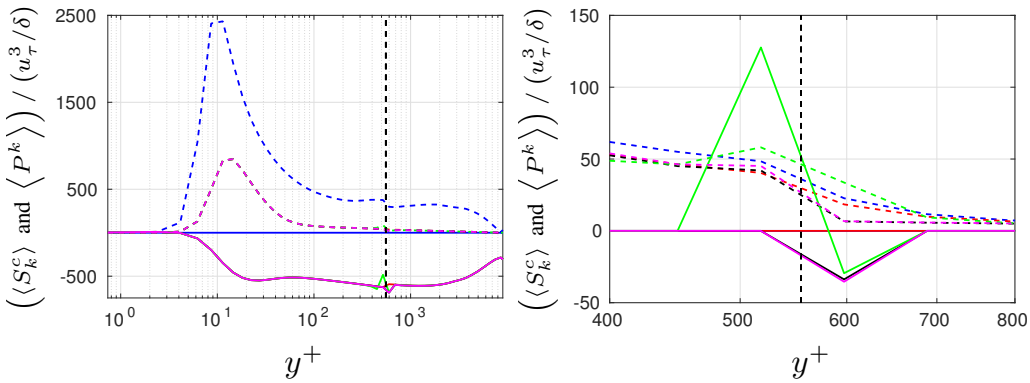

(a) At wall-normal the interface, $x/\delta = 0.925$. (b) At the wall-parallel interface, $x/\delta = 5.025$.

Figure 4.11: Channel flow using embedded LES, $Re_\tau = 8000$. Commutation (solid) and production (dashed) terms in the k equation. Dashed black line indicates the wall-parallel interface. In (a), the lines representing simulations with the commutation terms applied in the k, ω and momentum equations overlap. Colors as in Fig. 4.10.

4.5 Hump flow

The flow over a wall-mounted hump, as described in Fig. 4.12, is simulated using a two-stage semi-coupled embedded LES approach in order to evaluate the proposed modeling approach in separated flow. The flow is characterized by a large-scale separation on the lee side of the wall-mounted hump as well as a free shear layer emanating from the crest of the hump. The flow over the hump separates at $x\ /\ c = 0.65$ and reattaches at $x\ /\ c = 1.1$. The Reynolds number based on the free stream velocity and the hump chord is $Re_c = 936\ 000$.

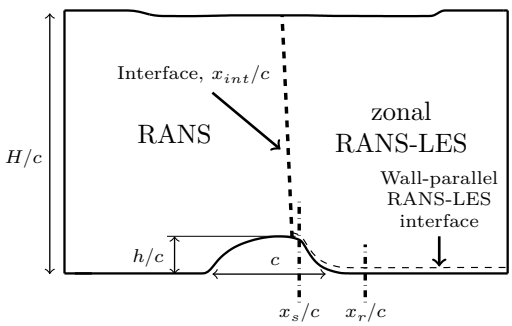

Figure 4.12: Hump configuration. Computational domain with interface ($x_{int}/c = 0.60$), flow separation ($x_s/c = 0.65$) and re-attachment ($x_r/c = 1.1$) lines. Not to scale.

Precursor RANS simulations of the whole domain were made using Menter's SST $k-\omega$ model (paper B, simulations performed by Prof. Strelets group in St. Peterburg) and the

PDH-LRN RANS model (paper D) from which the turbulent properties at the inlet were taken. The inlet velocity profiles were taken from a precursor embedded LES simulation performed by ANSYS. Synthetic turbulent fluctuations were applied at the inlet plane. A RANS layer is applied in the near-wall region, and the wall-parallel RANS-LES switch is prescribed at a specific grid line. Three different switch locations were evaluated: $j = 26$, 32 and 36, corresponding to $y^+ = 112$, 260 and 450, respectively, at the interface ($x/c = 0.60$). The LES length scale $\Delta = \Delta_{dw}$ was used in all simulations.

In paper B, the ratio of SGS to RANS turbulent kinetic energy was prescribed in the range $0.05 \leq f_{k,int} \leq 0.20$ and the synthetic turbulent fluctuations were scaled with the inlet turbulent kinetic energy profile. It was concluded in that paper that the level of $f_{k,int}$ at the inlet plane had only a minor effect on the downstream flow. In paper E, the commutation terms in the k and ω equations were applied at the inlet boundary and the fluctuations were scaled by the inlet shear stress profile from the precursor RANS simulation.

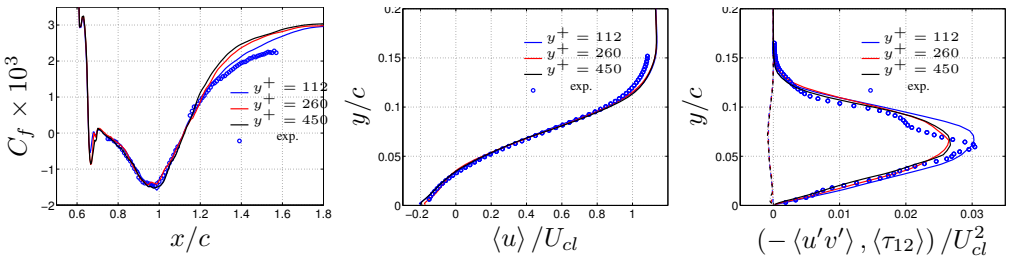

(a) Skin friction. (b) Streamwise velocity, $x/c = 1.0$. (c) Shear stress, $x/c = 1.0$.

Figure 4.13: Hump flow using embedded LES, $\Delta = \Delta_{dw}$. (a) Skin friction along the bottom wall. (b) Streamwise velocity. (c) Turbulent shear stress, resolved (solid line) modeled+viscous (dash-dotted line).

As can be seen in Fig. 4.13, where the interface methodology presented in paper D is applied, there is a general good agreement of the simulated flow and the experiment. The flow in the separated flow region agrees very well with the experimental data, whereas a small deviation in the skin friction is observed in the recovery region downstream of the flow separation. Almost negligible differences are observed in the predicted skin friction and the velocity profiles in the separated flow region between the different wall parallel RANS-LES interface locations. A slightly better prediction of the shear stress is given when the RANS-LES interface is prescribed at $y^+ = 112$, which is expected since more of the separated flow is simulated as LES. The small differences between the flow cases presented are due to the fact that the commutation terms at the inlet plane are also applied in the RANS region as motivated in Section 3.2.1. Even though only profiles at $x/c = 1.0$ are presented in this extended summary and in paper D, the profiles are very well captured in general in the whole domain with the proposed model.

4.6 Spatially developing boundary layer flow

Simulation of spatially developing boundary layers is essential in the aeronautical industry in order to achieve accurate predictions of aircraft drag. Moreover, the ability to accurately predict the resolved turbulence in the outer part of the boundary layer is important for predictions of shallow flow separation, typically present over the trailing edge of a wing, since the behaviour of those separations is strongly coupled to the upstream boundary layer turbulence. The spatially developing boundary layer is therefore simulated in this thesis with a wall-parallel RANS-LES interface located inside the boundary layer.

As for the hump flow, the spatially developing boundary layer flow is simulated using a two-stage semi-coupled embedded LES approach. The Reynolds number range covered by the simulations is approximately $3000 \leq Re_\theta = U_{inf}\theta/\nu \leq 6000$, where θ is the momentum thickness. Profiles of u, v, k and ω, from a precursor RANS simulation using the PDH-LRN model, are prescribed at the inlet boundary. The RANS values of the turbulent kinetic energy and the specific dissipation rate of k are manipulated at the inlet boundary using the commutation terms in the k and ω equations, as described in Section 3.2.1, in order to reach typical SGS levels. Synthetic turbulent fluctuations are imposed at the inlet boundary to obtain a rapid development of the downstream turbulence-resolving LES flow. The flow is simulated with a near-wall RANS layer and an off-wall LES region. The wall-parallel RANS-LES interface is located at $y^+ = 220$. The LES length scale $\Delta = \Delta_{dw}$ is used in all simulations.

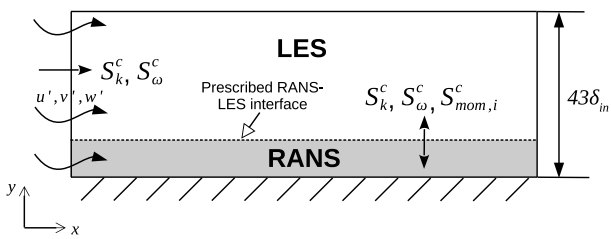

Figure 4.14: Schematic of the computational set-up for spatially developing boundary layer flow.

Two grids were used for the simulations. Grid 1 is designed by Onera in the EU-FP7 Go4Hybrid and the Garteur AG54 projects. The computational domain used consists of $(n_x, n_y, n_z) = (580, 124, 64)$ cells. The dimensions of the computational domain in the streamwise, spanwise and in the wall-normal directions are, respectively, $L_x/\delta_{in} = 102$, $L_z/\delta_{in} = 3.1$ and $L_y/\delta_{in} = 43$. The grid reads in viscous units $(\Delta x^+, \Delta y^+, \Delta z^+) = (114 - 230, 1 - 3688, 57)$. The grid is stretched in the streamwise direction so that $\Delta x/\Delta z = 2$ at the inlet and $\Delta x/\Delta z = 4$ at $x/\delta_{in} = 72$ ($Re_\theta = 6000$). Grid 2 uses the same node distribution in viscous units at the inlet as grid 1 but with a constant $\Delta x/\Delta z = 2$ in the streamwise direction in order to evaluate the influence of the growing $\Delta x/\Delta z$ used in grid 1. For grid 2, $(n_x, n_y, n_z) = (872, 124, 60)$. The simulated length is approximately $x/\delta_{in} = 72$ for both grids.

In paper E, where simulations with the two grids were compared, it was concluded that $\Delta x/\Delta z > 2$ should be avoided. With grid 1, where $2 \leq \Delta x/\Delta z \leq 4$, a much pronounce skin friction deviation was observed as compared to the Cole-Fernholz correlation, which was used as reference. This deviation was not observed with grid 2, where $\Delta x/\Delta z = 2$. The simulations presented in this extended summary and in paper F are therefore computed using grid 2.

From the skin friction coefficient presented in Fig. 4.15 (a), it can be concluded that the proposed model performs well. All simulations are within $\pm 5\%$ to the reference correlation for $Re_\theta > 4500$, irrespective of the methodology used at inlet boundary and the wall-parallel RANS-LES interface. Moreover, it can be concluded that it is preferable to apply the commutation terms in the k and ω equations at the inlet to achieve a more rapid re-establishment of the turbulence in the hybrid RANS-LES region. It is furthermore not recommended to apply the commutation terms in the k and ω equations on the RANS side of the wall parallel interface since this gives too low a skin friction compared to the reference correlation.

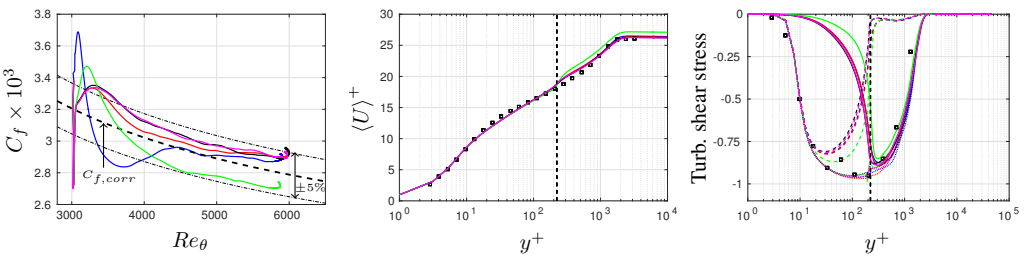

(a) Skin friction. (b) Stremwise velocity. (c) Turbulent shear stress.

Figure 4.15: Boundary layer. (a) Skin-friction distribution. (b) Streamwise velocity at $Re_\theta = 5200$. (c) Turbulent shear stress at $Re_\theta = 5200$. Markers are experimental data [64]. Vertical dashed black line indicates the wall-parallel interface.

The streamwise velocity and the turbulent shear stress at $Re_\theta = 5200$ are presented in Fig. 4.15 (b) and (c). Both the velocity profiles and the profiles of turbulent shear stress are in good agreement with the experimental data [64]. Because of $\Delta = \Delta_{dw}$, only a weak log-layer mismatch is observed. A slight over-prediction of the free stream velocity is seen for the simulation where the commutation terms are applied in the k and ω equations on both sides of the wall-parallel RANS-LES interface. This corresponds well to the lower skin friction predicted with this simulation. It can also be seen in Fig. 4.15 (c) that the slowest growth of the resolved turbulent shear stress is given in this simulation whereas the development of the resolved shear stress is similar in the other simulations.

4.7 Mixing layer flow

Mixing layer flows and free shear flows are often encountered in aeronautical applications. Examples of typical applications where mixing layers appear are jet flows, separated flow in aircraft inlets and over aircraft wings. In this thesis, the mixing layer flow, investigated

experimentally by Delville [65], has been simulated as a one stage fully coupled embedded LES, as shown in Fig. 4.16. The purpose of the flow case is to evaluate the grey area mitigation methodologies based on the commutation terms in the k, ω and momentum equations as presented in Section 3.2.1. Moreover, the effect of different LES length scales on the downstream development of LES resolved turbulence after the embedded RANS-LES interface is evaluated as is the effect of different discretization schemes.

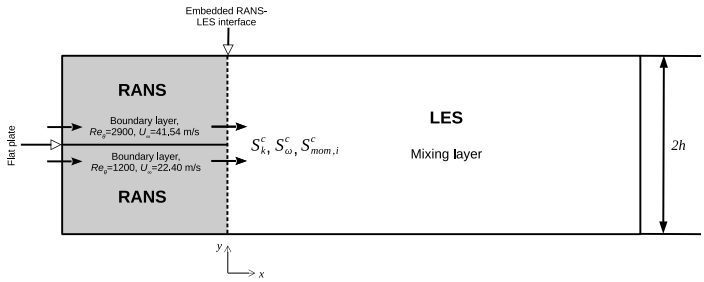

Figure 4.16: Mixing layer. Computational domain with embedded RANS-LES interface.

The computational domain includes an infinitely thin flat plate, with different boundary layers on each side, and the region downstream of the flat plate trailing edge where the two boundary layers mix. The technique used to simulate the infinitely thin flat plate was implemented in CALC-LES in Matsfelt [66]. The boundary layers on each side of the flat plate have different freestream velocities and different Reynolds numbers. The experimental boundary layer properties at the trailing edge are presented in Table 4.2.

The boundary layers on each side of the flat plate are simulated with RANS. The wall-normal embedded interface, where the simulation switches from RANS to LES, is located at the trailing edge of the flat plate. The mixing layer flow downstream of the trailing edge is simulated using LES. The inlet boundary layer profiles, applied on each side of the flat plate, have been computed in separate RANS boundary layer simulations to achieve similar boundary layer profiles at the trailing edge as in the reference experiment.

Table 4.2: Flow conditions of the boundary layers at $x = -10$ mm. Data from experiment [65].

Measure	Notation	High velocity BL	Low velocity BL
Velocity	U_∞	41.54 m/s	22.40 m/s
Thickness	δ	9.6 mm	6.3 mm
Displacement thickness	δ_1	1.4 mm	1.0 mm
Momentum thickness	θ	1.0 mm	0.73 mm
Shape factor	H	1.35	1.37
Re-number based on θ	Re_θ	2900	1200
Turbulence level	u'/U_∞	$\sim 0.3\%$	$\sim 0.3\%$

The grids used in the simulations are similar to the grids designed by NLR for the

FP7 Go4Hybrid project and the Garteur AG54 project. The grid on each side of the flat plate is symmetric with $y = 0$ located at the plate. The wall-normal grid resolves the boundary layers down to $y^+ = 1$. The flat plate has a length of 0.149 m, consisting of 20 cells in the streamwise direction, and the domain for the mixing layer downstream of the flat plate trailing edge is 1 m. In the simulations, $x = 0$ at the trailing edge of the flat plate. The height of the domain on each side of the flat plate is $h = 0.15$ m. The spanwise extension of the domain is $z_{\max} = 0.15$ m. In the mixing layer region, the mesh is equidistant in the streamwise x direction and the spanwise z direction. For the coarse and fine grids $\Delta x = \Delta z = 3.1250$ mm and 1.5625 mm, respectively. The computational domains have $(n_x, n_y, n_z) = (354, 146, 48)$ and $(674, 146, 96)$ cells, respectively.

The commutation terms in the k, ω and momentum equations are applied at the wall-normal embedded RANS-LES interface at $x = 0$ mm. As a reference, a simulation is used where no commutation terms are applied at the interface. This simulation is compared to simulations where the commutation terms are applied in the k and ω equations and in the k, ω and momentum equations, respectively. The LES length scale used in the simulations is Δ_{max} and Δ_Ω, see Eqs. (3.20) and (3.22).

The growth of the mixing layer thickness, expressed as vorticity thickness and momentum thickness, is presented in Fig. 4.17. The vorticity thickness and momentum thickness are defined in Eqs. (4.1) and (4.2).

$$\delta_\omega = \frac{U_a - U_b}{(\partial U/\partial y)_{y=0}} \tag{4.1}$$

$$\theta = \int_{-\infty}^{\infty} \frac{U - U_b}{U_a - U_b}\left(1 - \frac{U - U_b}{U_a - U_b}\right) dy \tag{4.2}$$

In Eqs. (4.1) and (4.2), U_a and U_b are taken as the streamwise velocity at $y = -h$ and $y = h$.

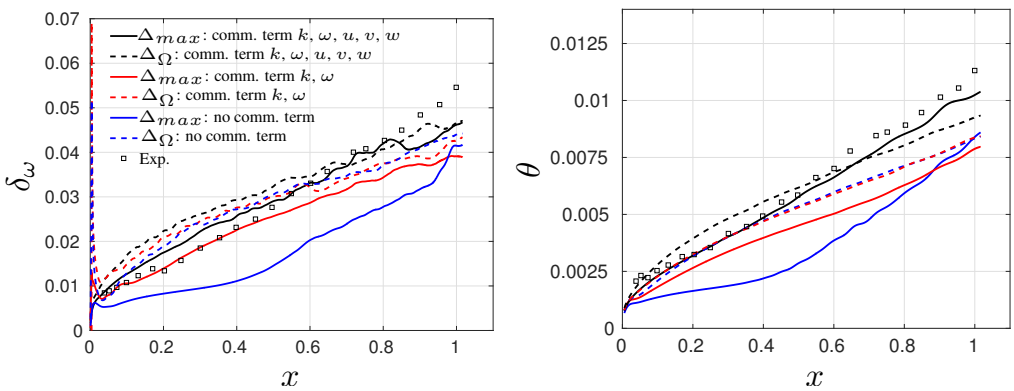

(a) Vorticity thickness.

(b) Momentum thickness.

Figure 4.17: Mixing layer. Growth of vorticity thickness and momentum thickness.

The grey area mitigation methodologies used are more decisive on the fine grid than

on the coarse grid, especially when $\Delta = \Delta_{max}$. Without any commutation terms at the RANS-LES interface and $\Delta = \Delta_{max}$, both the vorticity thickness and the momentum thickness are much under-predicted. Applying the commutation terms in the k and ω equations at the embedded interface, the results are improved using Δ_{max}. However, with the commutation terms also added in the momentum equations, both the vorticity thickness and the momentum thickness are much improved. With $\Delta = \Delta_{\Omega}$, the effect of the commutation terms at the RANS-LES interface is much weaker than for $\Delta = \Delta_{\max}$ on both grids. This is mainly due to the lower turbulent viscosity given by the vorticity based LES length scale, as seen in Fig. 4.18 (a), which contributes to a rapid formation of the resolved turbulence without any aid from the commutation terms.

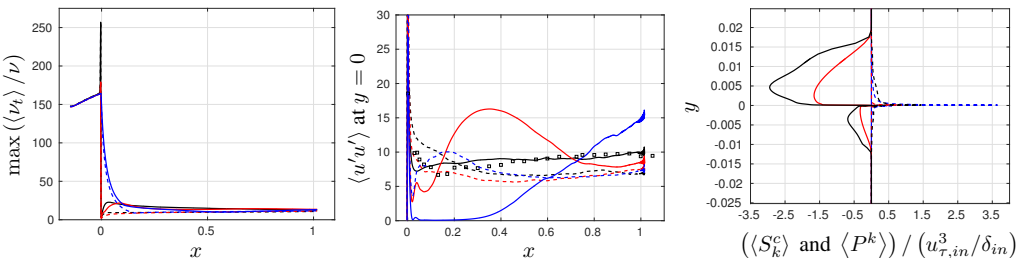

(a) $\max(\langle \nu_t \rangle / \nu)$. (b) $\langle u'u' \rangle$ at $y = 0$. (c) Commutation and production terms.

Figure 4.18: Mixing layer. Turbulent viscosity, resolved streamwise turbulent fluctuations along the x-direction and commutation terms in the k-equation. Colors as in Fig. 4.17.

The commutation term in the momentum equations, clearly act as a turbulence generator at the interface, as seen in Fig. 4.18 (b). With $S^c_{mom,i}$, the predicted turbulent normal stress in the streamwise direction is in very good agreement with the experimental data using Δ_{max} on both grids. The commutation term in the momentum equations also increases the production of the modeled turbulent kinetic energy at the interface. The peak in the turbulent viscosity at the interface shown in Fig. 4.18 (a) is thus due to the commutation term in the momentum equations. Owing to the same mechanism, there is a quicker growth of the SGS turbulent viscosity shortly downstream of the trailing edge with the commutation term applied in the momentum equations, compared to the simulation where the commutation terms are added only in the k and ω equations. Differences are also observed in the commutation terms in the k equation, as seen in Fig. 4.18 (c). With $S^c_{mom,i}$ applied, the magnitude of the commutation term in the k equation takes larger values than if the commutation terms are applied only in the k and ω equations.

It can be concluded that the proposed model, with the RANS-LES interface methodologies presented in this thesis, is able to predict the simulated mixing layer in reasonable agreement with experimental data. It has been shown that the LES length scale has a large impact on the extension of the RANS-to-LES transition region. However, it is not obvious that the LES length scale that gives the lowest turbulent viscosity (Δ_{Ω} in this thesis) is the best suited length scale to predict the simulated mixing layer flow. The overall prediction of the simulated mixing layer flow is best made using $\Delta = \Delta_{max}$ provided that the interface methodologies presented in this thesis are applied. Furthermore,

the discretization scheme used is critical. In all simulations presented in this extended summary, a second order central differentiating scheme (CDS) was used. Additional simulations have been made using a blend of 2% and 5% second order upwind scheme with 98% and 95% CDS, respectively. With the use of upwinding, almost no resolved turbulent stresses are developed with Δ_{max}, and the vorticity and the momentum thicknesses are much under-predicted. This suggests that the turbulence-resolving capability is very sensitive to numerical diffusion.

5 Summary of papers

This chapter briefly summarizes the work done in the papers appended in the thesis. Comments are also given to some of the papers to highlight possible improvements and future work.

5.1 Paper A

"Feasibility of Hybrid RANS-LES of Shock/Boundary-Layer Interaction in a Duct"

The paper presents an assessment of RANS and hybrid RANS-LES models applied to transonic flow in a rectangular duct. Two computational grids were used, one coarse and one refined. The main focus of the paper was to predict the shock/boundary-layer interaction (SBLI) and the corner separation bubbles induced by the shock at Mach 1.4 using hybrid RANS-LES methods.

All the hybrid RANS-LES models studied in the paper failed to capture the underlying physics of the shock-induced corner flow separation. The standing shock wave is collapsed in association with the prediction of the corner flow separation. One of the RANS models evaluated, the PDH-LRN model [48], predicted the SBLI flow in reasonably good agreement with the experimental data.

The modeling demands that special attention be paid to the RANS-LES interface in relation to the local grid resolution. Even in the SA-DDES model, the use of a shielding function is not justified in the region of the separation zone. The shielding function has played a role as desired in the boundary layer upstream of the SBLI zone but does not respond properly to the separated region, which predicted a much earlier onset of the corner flow separation and made the corner separation bubble largely over-predicted. The poorly predicted shock wave and corner separation bubble in the SA-DDES simulation is not only due to the DDES formulation but also to the underlying SA RANS model. The location of the simulated bubble onset is concluded to be very important and essential in the prediction of corner bubble size. Moreover, it is concluded that too early a predicted onset and an exaggerated corner bubble will break down the shock wave and form an unphysical re-compression shock.

The study of the current SBLI flow showed that a time step corresponding to an acoustic CFL number of 1 is required in the bulk flow at the shock for the grids used in order to capture the fluctuations in the SBLI zone. Using the refined grid, large differences were found in the prediction of the corner separation and shock intensity, as compared to the coarse grid.

Comments
None of the evaluated hybrid RANS-LES models gave results in reasonable agreement with experimental data. It was concluded that the modeling of the incoming boundary layer to the SBLI region and the corner separation bubbles must be improved as must also the LES predicted separated flow downstream of the shock. Due to the PDH-LRN RANS model's ability to predict the SBLI flow, it was chosen as the background RANS

model in the hybrid RANS-LES modeling development work presented in the subsequent papers appended to this thesis.

5.2 Paper B

"Hybrid RANS-LES Modeling Using a Low-Reynolds-Number $k-\omega$ Based Model"

With the knowledge gained from the work reported in paper A, paper B presents the derivation of the new hybrid RANS-LES model based on PDH-LRN. Moreover, the paper presents results of the calibration of the LES mode of the model which was done using Decaying Homogeneous Isotropic Turbulence (DHIT), giving the LES constant $C_{LES} = 0.70$. The proposed hybrid RANS-LES model was validated made in fully developed channel flow at $Re_\tau = 8000$, channel flow simulated with embedded LES at $Re_\tau = 950$ and in flow over a wall-mounted hump.

In simulations of fully developed channel flow, different LES length scales were evaluated in order to find possible solutions to reduce the log-layer mismatch, which is almost always present in hybrid RANS-LES simulations with the outer part of the boundary layer simulated with LES. The model's sensitivity to the location of the wall-parallel RANS-LES interface was also evaluated. It was concluded that the wall distance based LES length scale Δ_{dw} (see Eq. 3.23) substantially reduces the log-layer mismatch compared to other well established LES length scales used in the literature. Moreover, it was shown that there is a weak dependency on the location of the RANS-LES interface with respect to the log-layer mismatch for Δ_{dw}.

In the embedded LES simulations of channel flow, the upstream RANS region and the downstream LES region were simulated simultaneously and coupled with a wall-normal RANS-LES interface onto which synthetic turbulent fluctuations were added in order to reduce the transition region from RANS to LES. No near-wall RANS layer was applied in the LES region. Across the RANS-LES interface, the convective and diffusive fluxes of k and ω were manipulated to speed up the transition from RANS to LES. A ratio of modeled to resolved turbulent kinetic energy was prescribed at the RANS-LES interface. The ratio in the range $0.05 \leq f_{k,in} \leq 0.20$ was evaluated.

The hump flow was simulated as a two-stage semi-coupled embedded LES, where a precursor RANS simulation with Menter's SST $k-\omega$ (MSST) served as inlet boundary conditions for k and ω and a precursor embedded LES simulation served with boundary conditions for the velocities. Synthetic turbulent fluctuations were applied at the inlet plane and the ratio of modeled to resolved turbulent kinetic energy was prescribed as in the above simulations of channel flow.

The flow fields from the embedded LES simulations of channel flow and hump flow agree reasonably well with available DNS data (channel flow) and experimental data (hump flow). For the hump flow, an additional simulation was made with MSST as the background RANS model for reference. It was concluded that using PDH-LRN and MSST as background RANS models give similar predictions of the flow.

It can thus be concluded from paper B that, with the use of Δ_{dw} in the proposed hybrid RANS-LES model, channel flow can be well predicted. Moreover, the paper shows

that the proposed hybrid RANS-LES model is able to predict the separated flow on the lee side of the wall-mounted hump.

5.3 Paper C

"Prediction of Transonic Duct Flow Using a Zonal Hybrid RANS-LES Modeling Approach"

In the work reported in paper C, the hybrid RANS-LES model presented in paper B is applied to the transonic duct flow, with SBLI described in paper A, using a zonal approach. The flow domain upstream of the SBLI region are simulated with RANS whereas the SBLI region and the subsequent flow is simulated as hybrid RANS-LES with a prescribed near-wall RANS layer and an off-wall LES region. Upstream of the SBLI region, a buffer zone is patched in which the turbulent length scale is blended in the streamwise direction from its RANS level to its LES level in order to avoid possible discontinuities in the transition from RANS to LES. Simulations of the proposed model are compared to Spalart-Allmaras based DDES and IDDES, the PDH-LRN RANS model and to experimental data.

The simulations clearly indicate that the onset of the corner separation bubble relative to the shock location is one of the key issues for accurately predicting the SBLI flow. The incoming boundary layer, the shock intensity and the shock foot shape are also closely interconnected, and an accurate prediction of these SBLI flow properties is shown to be challenging using hybrid RANS-LES simulations.

The proposed hybrid RANS-LES model produced a λ-shape shock foot and a pressure rise across the shock, which are in reasonable agreement with experimental data. The simulation has slightly exaggerated the corner separation bubbles, which subsequently led to a more pronounced cross flow.

The paper reports large differences in how the models have simulated the corner flows. The SA-IDDES model adapted reasonably well to the recirculating flow and resolved a large part of the corner flow in LES mode. On the other hand, the SA-DDES model, produced high levels of turbulent viscosity in the corner separation bubbles and much less resolved turbulent structures. As compared to the PDH-LRN based HRLM and the experimental data, the SA-IDDES predicted a weaker λ-foot, which caused a slightly less distinct pressure rise in the wall pressure distribution across the shock. In the zonal simulations with the proposed model, the RANS and LES zones were prescribed so that the outer part of the corner separation bubbles were simulated in LES mode, which seems advantageous for the grid used, as this gave an improved prediction of the SBLI flow.

Comments
The motivation for using the zonal approach presented in the paper was to ensure an accurate modeling of the attached boundary layer flow upstream of the SBLI region. This was achieved with RANS. However, since the corner separation bubbles are partly embedded in the incoming boundary layer, it would be advantageous to trigger resolved turbulence in the boundary layer upstream of the shock, e.g. by adding synthetic turbulent fluctuations, to improve the prediction of the flow in the subsequent SBLI region. Even though the blending function, used to avoid discontinuities is the modeled turbulent

quantities, rapidly switches the turbulent length scale from RANS to LES it contributes to delay the development of resolved turbulence compared to when the turbulent length scale is switched across a single grid plane.

In some of the presented simulations, large scale turbulent structures, emanating from the interaction between the shock wave and the corner flow separations, caused pressure fluctuations and high local velocities at the outlet boundary. To avoid such fluctuations and thereby speed up the convergence in each time step, it is recommended to extend the duct further downstream of the SBLI region so that no large scale turbulence is present at the outlet boundary.

5.4 Paper D

"Hybrid Reynolds-Averaged Navier-Stokes/Large-Eddy Simulation Modeling Based on a Low-Reynolds-Number $k-\omega$ Model"

This paper describes improved predictions of the embedded LES simulated channel flow at $Re_\tau = 950$ and the hump flow. Results of fully developed channel flow at $Re_\tau = 8000$ from paper B are also included.

Compared to the simulations of channel flow and hump flow simulated as embedded LES presented in paper B, the wall-normal RANS-LES interface methodology is changed. The RANS-LES interface methodology used in this paper is based on commutation terms as in Hamba [38] instead of the prescribed ratio of modeled to resolved turbulent kinetic energy used in paper B. With commutation terms at the wall-normal RANS-LES interface in channel flow and the inlet plane in the hump flow, the use of "free" empirical constants is eliminated. Moreover, the synthetic inlet fluctuations are scaled with the turbulent shear stress profile. The integral length scale needed for the generation of synthetic turbulent fluctuations is computed in this paper as the maximum turbulent length scale at the inlet/RANS-LES interface based on k and ω from a precursor RANS simulation. In paper B, the length scales were computed as $l_{t,s} = 0.3\delta_{in}$, where δ_{in} is the boundary layer thickness of the incoming flow.

With the new RANS-LES interface methodology, the prediction of the resolved turbulent stresses was improved in comparison with the data given in paper B for both the channel flow and the hump flow. Moreover, the skin friction and the velocity profiles predicted in the flow separation region of the hump flow were in very good agreement with experimental data.

5.5 Paper E

"Grey-area mitigation using commutation terms at the interfaces in hybrid RANS-LES modeling"

The paper presents simulations, using the proposed hybrid RANS-LES model, of fully developed channel flow at $Re_\tau = 8000$ and spatially developing boundary layer flow in the range $3000 \leq Re_\theta \leq 6000$ with commutation terms also introduced at the wall-parallel

RANS-LES interfaces. The commutation terms are introduced in the k, ω and momentum equations at the RANS-LES interfaces with the aim of mitigating the grey area. Four different LES length scales were evaluated together with the commutation terms in the k and ω equations in fully developed channel flow.

It is concluded that, for flows where the mean flow aligns with the RANS-LES interface, the effect of the proposed commutation terms, with respect to the mitigation of the grey area, is weak. Moreover, it is concluded from simulations of fully developed channel flow that the choice of LES length scale has a much stronger effect on the mitigation of the log-layer mismatch than does the addition of commutation terms.

In the simulations of spatially developing boundary layer flow that are presented, it is shown that the commutation terms in the k and ω equations applied at the inlet are needed in order to allow the LES simulated flow to recover a physical skin friction distribution. A weaker effect of the commutation terms applied at the wall parallel interface is observed on the skin-friction distribution. Moreover, two grids have been used with different cell stretching in the streamwise direction, $2 \leq \Delta x/\Delta z \leq 4$ and $\Delta x/\Delta z = 2$ (same Δz is used for both grids) and it is concluded that for $\Delta x/\Delta z > 2$, the predicted C_f-distributions do not align well with the Fernholz-Coles correlation for the simulated Reynolds number range.

5.6 Paper F

"A hybrid RANS-LES interface method for grey-area mitigation in turbulence-resolving simulations"

In paper F, the low-Reynolds-number $k-\omega$ based hybrid RANS-LES turbulence model was used to evaluate the effect of commutation terms at the RANS-LES interfaces, in order to mitigate the grey area. The proposed methodology is evaluated in embedded LES simulations of channel flow, boundary layer flow and mixing layer flow. The commutation terms were applied to the convection terms in the k, ω and momentum equations at wall normal and wall parallel RANS-LES interfaces. The LES length scale Δ_{max} and Δ_Ω are evaluated for the mixing layer flow.

The effect of the commutation terms in the k and ω equations is to reduce the turbulent viscosity on the LES side of the interface and increase the turbulent viscosity on the RANS side of the RANS-LES interface. The commutation terms in the momentum equations act as a turbulence generator in order to compensate the reduction of the modeled turbulent kinetic energy with resolved turbulent kinetic energy across the RANS-to-LES interface.

At the wall-normal embedded interface in the channel flow simulations and at the inflow boundary in the boundary layer simulations, the commutation terms in the k and ω equations are applied along with synthetic turbulent fluctuations. Commutation terms in the k, ω and momentum equations are applied at the embedded interface in the mixing layer flow without any synthetic turbulent fluctuations.

In all three flow cases presented, the commutation terms in the k and ω equations applied to the wall-normal interfaces rapidly reduce the turbulent viscosity. It is also concluded that the magnitude of the commutation term at these interfaces in the k

equation is much larger than the magnitude of the production term. At the wall-parallel RANS-LES interfaces (channel flow and boundary layer flow), the magnitudes of the commutation and production terms in the k equation are the same.

The effect on the RANS-to-LES transition region due to the introduction of the commutation terms at the LES inlet is much weaker in the channel flow simulations than in the boundary layer simulations. In the boundary layer simulations, the different wall parallel interface methods give clear differences in the predicted skin friction distributions. The shortest recovery length with a reasonably well predicted skin friction level is given when no commutation terms are applied at the wall-parallel interface. However, all the simulations predict a skin friction distribution within 5% compared to the Coles-Fernholz correlation, which was used as the reference.

With the use of the commutation terms in the k, ω and momentum equations at the embedded interface in the mixing layer simulations, a capability to quickly establish accurate resolved stresses was proven in the paper. It can be concluded that the commutation terms in the k and ω equations reduce the turbulent viscosity at the trailing edge of the flat plate. However, this is not sufficient to achieve a rapid start-up of the resolved turbulence immediately downstream of the flat plate trailing edge using $\Delta = \Delta_{max}$. The turbulent fluctuations generated with the commutation terms in the momentum equations are needed to reduce the grey area. Since Δ_Ω produces a lower turbulent viscosity at the trailing edge of the flat plate, a more rapid development of the resolved turbulence is observed with this length scale, and the effect of the commutation term in the momentum equations is weaker. Moreover, it is concluded that the choice of discretization scheme is critical for an accurate prediction of the simulated mixing layer. A pure central scheme is needed to prevent damping of the developing natural instabilities in the mixing layer simulations. With a blend of a 5% second order upwind scheme with a 95% central scheme, only weak or resolved turbulent stresses were developed, and the growth rate of the mixing layer is much delayed.

6 Concluding remarks

A low-Reynolds-number $k-\omega$ based hybrid RANS-LES model is developed and verified with an emphasis on the exploration of the inherent RANS-LES interface methodologies for grey-area mitigation and log-layer mismatch reduction with the aim to improve predictions of complex turbulent flows, typically observed in aeronautical applications. The RANS-LES interface methodologies are based on commutation terms for the convection term in the k, ω and momentum equations as well as synthetic turbulent fluctuations. The grey area mitigation methodology explored does not involve any "free" empirical constants and is not tuned for the turbulence model used in the simulations presented.

The hybrid RANS-LES approaches proposed were applied to decaying homogeneous isotropic turbulence (DHIT) and channel flow for calibration purposes. Moreover, simulations of flow over a wall-mounted hump, spatially developing boundary layer flow, plane mixing layer flow and flow in a duct involving shock/boundary-layer interaction with local corner flow separations were successfully performed with results in good agreement with experimental data. The characteristic physics of the flows mentioned and the associated turbulence modeling challenges are all good representatives for the CFD challenges present in the design and analysis of existing and future aeronautical applications.

The proposed hybrid RANS-LES model was implemented in the structured incompressible flow solver CALC-LES and in the unstructured compressible flow solver Edge. The assessments of the proposed RANS-LES interface methodologies were made in CALC-LES.

With the use of commutation terms at the RANS-LES interface in the k and ω equations, it was shown that k and ω can be rapidly adapted from their RANS level to their subgrid scale (SGS) level on the LES side of the interface, giving an SGS adapted turbulent viscosity. Moreover, for a flow passing across the interface from LES to RANS, it was shown that the commutation terms in the k and ω equations contribute to an increased turbulent viscosity on the RANS side of the interface. With a commutation term also introduced in the momentum equations, which together with the commutation term in the k equation represents the transfer of energy between modeled and resolved turbulent scales, it has been shown that the RANS-LES methodology explored is able to trigger the equations to resolve turbulence and thus reduce the RANS-to-LES transition region.

When combining synthetic turbulent fluctuations with commutation terms in the k and ω equations at the inlet section in simulations of spatially developing boundary layer flow, it is concluded that the RANS-to-LES transition region is substantially reduced compared to when no commutation terms are used. The predicted skin-friction distribution in the boundary layer simulations deviated less then 5% from the Coles-Fernholz correlation used as a reference. This simulation approach was also successfully applied to the flow over the wall-mounted hump. In embedded LES simulations of plane mixing layer flow, the use of commutation terms in the k and ω equations, as well as in the momentum equations (without any synthetic turbulent fluctuations) at the wall-normal RANS-LES interface located at the flat plate trailing edge, gave a quick development of the resolved turbulence with resolved streamwise normal stresses in very good agreement with experimental data. However, a less clear advantage of the commutation terms applied at the wall-normal

RANS-LES interface, with respect to grey-area mitigation, was observed in the embedded LES simulations of channel flow at $Re_\tau = 8000$.

Four LES length scales from the literature were evaluated in fully developed channel flow, with the conclusion that the wall distance based LES length scale by Shur et al. [12] is superior in reducing the log-layer mismatch. It was further concluded that the effect of the commutation terms applied at the wall-parallel RANS-LES interface is weaker than on the wall normal interfaces. In addition, the choice of LES length scale has a much greater effect on the log-layer mismatch than the introduction of commutation terms at the wall-parallel RANS-LES interface.

Future challenges in hybrid RANS-LES modeling are strongly related to a further understanding of the coupling between the RANS and the LES simulated flows and how this can be improved to serve industrial aeronautical needs. This thesis contributes hybrid RANS-LES methodologies in the direction of industrial needs. The robustness and accuracy of the proposed approaches have been demonstrated, which are essential in achieving a more simulation-based design and analysis process for the aeronautical industry. This gives the possibility to reduce the use of costly wind tunnel tests and full scale flight tests.

References

[1] L. Davidson. *An Introduction to Turbulence Models*. Research report 97:2. Department of Thermo and Fluid Dynamics, Chalmers University of Technology, 2016.

[2] M. Lee and R. Moser. Direct numerical simulation of turbulent channel flow up to $Re \approx 5200$. *Journal of Fluid Mechanics* **774** (2015), pp. 395–415. DOI: 10.1017/jfm.2015.268.

[3] P. Schlatter and R. Örlü. Assessment of direct numerical simulation data of turbulent boundary layers. *Journal of Fluid Mechanics* **659** (2010), pp. 116–126.

[4] P. Spalart. Strategies for turbulence modelling and simulations. *International Journal of Heat and Fluid Flow* **21**.3 (2000), pp. 252–263. ISSN: 0142-727X. DOI: https://doi.org/10.1016/S0142-727X(00)00007-2. URL: http://www.sciencedirect.com/science/article/pii/S0142727X00000072.

[5] P. R. Spalart and V. Venkatakrishnan. On the role and challenges of CFD in the aerospace industry. *The Aeronautical Journal* **120**.1223 (2016), pp. 209–232.

[6] P. Spalart, W.-H. Jou, M. Strelets, and S. Allmaras. "Comments on the Feasability of LES for Wings, and on a Hybrid RANS/LES Approach". *Advances in DNS/LES*. Ruston, Lousiana, 1997, pp. 137–147.

[7] L. Davidson and S.-H. Peng. Hybrid LES-RANS modelling: a one-equation SGS model combined with a $k-\omega$ model for predicting recirculating flows. *International Journal for Numerical Methods in Fluids* **43** (2003), pp. 1003–1018.

[8] J. Kok, H. Dol, B. Oskam, and H. van der Ven. *Extra-Large Eddy Simulation of Massively Separated Flows*. AIAA 2004-0264, Reno, Nevada. 2004.

[9] S. Deck. Zonal-Detached-Eddy Simualtion of the Flow Around a High-Lift Configuration. *AIAA Journal* **43** (2005), pp. 2372–2384.

[10] S.-H. Peng. "Hybrid RANS-LES modelling based on zero- and one-equation models for turbulent flow simulation". *In Proceedings of 4th Int. Symp. Turb. and Shear flow Phenomena*. Vol. 3. Begell house, 2005, pp. 1159–1164.

[11] P. Spalart, S. Deck, M. Shur, K. Squires, M. K. Strelets, and A. Travin. A new version of detached-eddy simulation, resistant to ambiguous grid densities. *Theory of Computational Fluid Dynamics* **20** (2006), pp. 181–195.

[12] M. Shur, P. Spalart, M. Strelets, and A. Travin. A hybrid RANS-LES approach with delayed-DES and wall-modelled LES capabilities. *International Journal of Heat and Fluid Flow* **29** (2008), pp. 1638–1649.

[13] S. Girimaji. Partiall-Averaged Navier-Stokes model for turbulence: a Reynolds-averaged Navier-Stokes to direct numerical simulation bridging method. *Journal of Fluids Engineering* **73** (2006), pp. 413–421.

[14] B. Chaouat and R. Schiestel. A new integrated transport model for subgrid-scale stresses and dissipation rate for turbulent developing flows. *Physics of Fluids* **17** (2005).

[15] F. Menter and Y. Ergorov. The Scale-Adaptive Simulation Method for Unsteady Turbulent Flow Predictions. Part 1: Theory and Model Description. *Flow, Turbulence and Combustion* **85** (2010), pp. 113–138.

[16] J. Yan, C. Mockett, and F. Thiele. Investigation of Alternative Length Scale Substitutions in Detached-Eddy Simulation. *Flow, Turbulence and Combustion* **74** (2005), pp. 85–102.

[17] W. C.W. Reassessment of the Scale-Determinig Equation for Advanced Turbulence Models. *AIAA Journal* **26** (1988), pp. 1299–1310.

[18] S. J. General Circulation Experiments with the Primitive Equations. *Monthly Weather Review* **91** (1963), pp. 99–165.

[19] M. Strelets. *Detached Eddy Simulation of Massively Separated Flows*. AIAA 2001-0879, Reno, Nevada. 2001.

[20] P. Spalart and S. Allmaras. A One-Equation Turbulence Model for Aerodynamic Flows. *La Recherche Aérospatiale, 1, p. 5-21* **1** (1994), pp. 5–21.

[21] F. Menter. Two-Equation Eddy-Viscosity Turbulence Models for Engineering Applications. *AIAA Journal* **32** (1994), pp. 1598–1605.

[22] F. Menter and M. Kuntz. "Adaption of turbulence models to unsteady separated flow behind vehicles". *The aerodynamics of heavy vehicles: trucks, buses and trains*. Ed. by R. McCallen, F. Browand, and J. Ross. Berlin Heidelberg: Springer-Verlag, 2004.

[23] M. Gritskevich, A. Garbaruk, J. Schütze, and F. Menter. Development of DDES and IDDES Formulations for the $k-\omega$ Shear Stress Transport Model. *Flow, Turbulence and Combustion* **88** (2012), pp. 431–449.

[24] J. Kok. Resolving the dependence on freestream values for the $k-\omega$ turbulence model. *AIAA Journal* **38** (2000), pp. 1292–1295.

[25] M. L. Shur, P. R. Spalart, M. K. Strelets, and A. K. Travin. Synthetic Turbulence Generators for RANS-LES Interfaces in Zonal Simulations of Aerodynamic and Aeroacoustic Problems. *Flow, Turbulence and Combustion* **93**.1 (2014), pp. 63–92. ISSN: 1573-1987. DOI: 10.1007/s10494-014-9534-8. URL: http://dx.doi.org/10.1007/s10494-014-9534-8.

[26] P. Quéméré and P. Sagaut. Zonal multi-domain RANS/LES simulations of turbulent flows. *International Journal for Numerical Methods in Fluids* **40**.7 (2002), pp. 903–925. ISSN: 1097-0363. DOI: 10.1002/fld.381. URL: http://dx.doi.org/10.1002/fld.381.

[27] M. Terracol. A Zonal RANS/LES Approach for Noise Sources Prediction. *Flow, Turbulence and Combustion* **77**.1 (2006), pp. 161–184. ISSN: 1573-1987. DOI: 10.1007/s10494-006-9042-6. URL: http://dx.doi.org/10.1007/s10494-006-9042-6.

[28] I. Mary. "RANS/LES Simulation of a Separated Flow in a 3D Curved Duct". *Progress in Hybrid RANS-LES Modelling: Papers Contributed to the 3rd Symposium on Hybrid RANS-LES Methods, Gdansk, Poland, June 2009*. Ed. by S.-H. Peng, P. Doerffer, and W. Haase. Berlin, Heidelberg: Springer Berlin Heidelberg, 2010, pp. 205–211. ISBN: 978-3-642-14168-3. DOI: 10.1007/978-3-642-14168-3_17. URL: http://dx.doi.org/10.1007/978-3-642-14168-3_17.

[29] S. Deck. Recent improvments in the Zonal Detached Eddy Simualtion (ZDES) formulation. *Theoretical and Computational Fluid Dynamics* (2011).

[30] N. Chauvet, S. Deck, and L. Jaquin. Zonal Detached Eddy Simualtion of a Controlled Propulsive Jet. *AIAA Journal* **45** (2007), pp. 2458–2473.

[31] Q. Zhang, W. Schröder, and M. Meinke. A zonal RANS-LES method to determine the flow over a high-lift configuration. *Computers & Fluids* **39**.7 (2010), pp. 1241–1253. ISSN: 0045-7930. DOI: http://doi.org/10.1016/j.compfluid.2010.02.006. URL: http://www.sciencedirect.com/science/article/pii/S0045793010000496.

[32] L. Davidson and S.-H. Peng. Embedded Large-Eddy Simulation Using the Partially Averaged Navier-Stokes Model. *AIAA Journal* **51** (2013), pp. 1066–1079.

[33] J. Ma, S.-H. Peng, L. Davidson, and F. Wang. A low Reynolds number variant of partially-averaged Navier-Stokes model for turbulence. *International Journal of Heat and Fluid Flow* **32** (2011), pp. 652–669.

[34] M. Billson, L.-E. Eriksson, and L. Davidson. *Modeling of Synthetic Anisotropic Turbulence and Its Sound Emission*. AIAA 2004-2857, 10th AIAA/CEAS Aeroacoustics Conference. 2004.

[35] L. Davidson and M. Billson. "Hybrid LES-RANS using synthesized turbulence for forcing at the interface". *ECCOMAS 2004*. Ed. by N. P., R. T., K. S., O. E., P. J., and Knörzer. 2004.

[36] N. Nikitin, F. Nicoud, B. Wasistho, K. Squires, and P. Spalart. An approach to wall modeling in large-eddy simulations. *Physics of Fluids* **12** (2000), pp. 1629–1632.

[37] L. Davidson and S. Dahlström. Hybrid RANS-LES: an approach to make LES applicable at high Reynolds number. *International Journal of Computational Fluid Dynamics* **19**.6 (2005), pp. 415–427.

[38] F. Hamba. Analysis of filtered Navier-Stokes equation for hybrid RANS/LES simulation. *Physics of Fluids A* **23** (2011).

[39] S. Girimaji and S. Wallin. Closure modeling in bridging regions of variable-resolution (VR) turbulence computations. *Journal of Turbulence* **14**.1 (2013), pp. 72–98. DOI: 10.1080/14685248.2012.754893. eprint: http://dx.doi.org/10.1080/14685248.2012.754893. URL: http://dx.doi.org/10.1080/14685248.2012.754893.

[40] L. Davidson. Zonal PANS: evaluation of different treatments of the RANS-LES interface. *Journal of Turbulence* **17**.3 (2016), pp. 274–307.

[41] L. Davidson. Two-equation hybrid RANS-LES models: a novel way to treat k and ω at inlets and at embedded interfaces. *Journal of Turbulence* **18**.4 (2017), pp. 291–315.

[42] M. Breuer, N. Joicic, and K. Mazaev. Comparison of DES, RANS and LES for the separated flow around a flat plate at high incidence. *International Journal for Numerical Methods in Fluids* **41** (2003), pp. 357–388.

[43] C. Mockett, M. Fuchs, A. Garbaruk, M. Shur, P. Spalart, M. Strelets, F. Thiele, and A. Travin. "Two Non-zonal Approaches to Accelerate RANS to LES Transition of Free Shear Layers in DES". *Progress in Hybrid RANS-LES Modelling*. Ed. by S. Girimaji, W. Haase, S.-H. Peng, and D. Schwamborn. Vol. 130. NNFM. Cham: Springer International Publishing, 2015, pp. 187–201. ISBN: 978-3-319-15141-0. DOI: 10.1007/978-3-319-15141-0_15. URL: http://dx.doi.org/10.1007/978-3-319-15141-0_15.

[44] M. L. Shur, P. R. Spalart, M. K. Strelets, and A. K. Travin. An Enhanced Version of DES with Rapid Transition from RANS to LES in Separated Flows. *Flow, Turbulence and Combustion* **95**.4 (2015), pp. 709–737. ISSN: 1573-1987. DOI: 10.1007/s10494-015-9618-0. URL: http://dx.doi.org/10.1007/s10494-015-9618-0.

[45] J. Kok and H. van der Ven. *Capturing free shear layers in hybrid RANS-LES simulations of separated flow*. Technical Report NLR-TP-2012-333. N, 2012.

[46] S.-H. Peng and L. Davidson. "Approximation of subgrid-scale stresses based on the Leonard expansion". *Turbulence, Heat and Mass Transfer 6*. 2009.

[47] S.-H. Peng. "Hybrid RANS-LES modelling with an energy backscatter function incorporated in the LES mode". *Proceedings of the Seventh International Symposium On Turbulence, Heat and Mass Transfer*. 2012.

[48] S.-H. Peng, L. Davidson, and S. Holmberg. A Modified Low-Reynolds-Number $k-\omega$ Model for Recirculating Flows. *Journal of Fluids Engineering* **119** (1997), pp. 867–875.

[49] P. Emvin. "The full multigrid method applied to turbulent flow in ventilated enclosures using structured and unstructured grids". PhD thesis. Chalmers University of Technology, 1997.

[50] P. Eliasson. *EDGE, a Navier-Stokes Slover for Unstructured Grids*. Scientific report FOI-R-0298-SE. C, 2001.

[51] C. W. Wilcox. Simulation of Transition with a Two-Equation Turbulence Model. *AIAA Journal* **32** (1994), pp. 247–255.

[52] C. Mocket. "A comprehensive study of detached-eddy simulation". PhD thesis. der Technischen Universität Berlin, 2009.

[53] S. Arvidson. *Assessment and Some Improvements of Hybrid RANS-LES Methods*. Licenciate thesis ISSN 1652-8565, 2013:01. Applied Mechanics, Chalmers University of Technology, 2013.

[54] P. Spalart. Detached-Eddy Simulation. *Annual Review of Fluid Mechanics* **41** (2009), pp. 181–202.

[55] F. Hamba. Log-layer mismatch and commutation error in hybrid RANS/LES simulation of channel flow. *International Journal of Heat and Fluid Flow* **30** (2009), pp. 20–31.

[56] L. Davidson. "Two-equation hybrid RANS-LES Models: A novel way to treat k and ω at the inlet". *Turbulence Heat and Mass Transfer, THMT-15*. Ed. by H. K. et al. Begell House Inc., New York, 2015.

[57] L. Davidson. Using Isotropic Synthetic Fluctuations as Inlet Boundary Conditions for Unsteady Simulations. *Adv Appl Fluid Mech.* **1**.1 (2006), pp. 1–3.

[58] S. Wallin and A. Johansson. An explicit algebraic Reynolds stress model for incompressible and compressible turbulent flows. *Journal of Fluid Mechanics* **403** (2000), pp. 89–132.

[59] P. J. K. Bruce and H. Babinsky. Unsteady shock wave dynamics. *Journal of Fluid Mechanics* **603** (2008), pp. 463–473.

[60] P. Bruce, H. Babinsky, B. Tartinville, and C. Hirsch. Corner Effect and Asymmetry in Transonic Channel Flows. *AIAA Journal* **49** (2011), pp. 2382–2392.

[61] H. A. New Advanced $k-\omega$ Turbulence Model for High-Lift Aerodynamics. *AIAA Journal* **43** (2005), pp. 1857–1869.

[62] G. Comte-Bellot and S. Corrsin. Simple Eularian Time Correlation of Full- and Narrow-Band Velocity Signals in Grid-Generated Isotropic Turbulence. *Journal of Fluid Mechanics* **48**.2 (1971), pp. 273–337.

[63] U. Bunge, C. Mockett, and F. Thiele. *Calibration of different models in the context of detached-eddy simulation*. Arbetisgemeinschaft "Strömmungen mit Ablösung" STAB Jahersbericht. 2003.

[64] D. DeGraaff and J. Eaton. Reynolds number scaling of the flat-plate turbulent boundary layer. *Journal of Fluid Mechanics* **422** (2000), pp. 319–346.

[65] J. Delville. "La décomposition orthogonale aux valeurs propres et l'analyse de l'organisation tridimensionnelle des écoulements turbulents ci saillés libres". PhD thesis. Université de Poitiers, 1995.

[66] J. Matsfelt. *Actuator turbine models and trailing edge flow: implementation in an in-house code*. Master thesis 2015:76. Applied Mechanics, Chalmers University of Technology, 2015.

[67] S. Arvidson, S.-H. Peng, and L. Davidson. "Feasibility of Hybrid RANS-LES of Shock/Boundary-Layer Interaction in a Duct". *Progress in Hybrid RANS-LES Modelling*. Ed. by F. S. et al. Vol. 117. NNFM. Springer, 2012, pp. 245–256.

[68] S. Arvidson, L. Davidson, and S.-H. Peng. *Hybrid RANS-LES Modeling Using a Low-Reynolds-Number $k-\omega$ Based Model*. AIAA paper 2014-0225, National Harbour, Maryland. 2014.

[69] S. Arvidson, S.-H. Peng, and L. Davidson. "Prediction of Transonic Duct Flow Using a Zonal Hybrid RANS-LES Modeling Approach". *Progress in Hybrid RANS-LES Modelling*. Ed. by S. G. et al. Vol. 130. NNFM. Springer, 2015, pp. 229–241.

[70] S. Arvidson, L. Davidson, and S.-H. Peng. Hybrid Reynolds-Averaged Navier-Stokes/Large-Eddy Simulation Modeling Based on a Low-Reynolds-Number $k-\omega$ Model. *AIAA Journal* **54** (2016), pp. 4032–4037. URL: `http://dx.doi.org/10.2514/1.J054179`.

[71] S. Arvidson, L. Davidson, and S.-H. Peng. "Grey-area mitigation using commutation terms at the interfaces in hybrid RANS-LES modeling". *To be published in Progress in Hybrid RANS-LES Modelling*. NNFM. Springer, 2017.

[72] S. Arvidson, L. Davidson, and S.-H. Peng. *Hybrid RANS-LES interface methods for grey-area mitigation in turbulence-resolving simulations*. Research report 2017:03. Applied Mechanics, Chalmers University of Technology, 2017.